

SLAC-PUB 14661
 IPPP/11/67
 DCPT/11/134
 LPN11-58
 FR-PHENO-2011-019
 MCNET-11-24

A critical appraisal of NLO+PS matching methods

Stefan Höche¹, Frank Krauss², Marek Schönherr², Frank Siegert³

¹ SLAC National Accelerator Laboratory, Menlo Park, CA 94025, USA

² Institute for Particle Physics Phenomenology, Durham University, Durham DH1 3LE, UK

³ Physikalisches Institut, Albert-Ludwigs-Universität Freiburg, D-79104 Freiburg, Germany

Abstract: In this publication, uncertainties in and differences between the MC@NLO and POWHEG methods for matching next-to-leading order QCD calculations with parton showers are discussed. Implementations of both algorithms within the event generator SHERPA are employed to assess the impact on a representative selection of observables. In the MC@NLO approach a phase space restriction has been added to subtraction and parton shower, which allows to vary in a transparent way the amount of non-singular radiative corrections that are exponentiated. Effects on various observables are investigated, using the production of a Higgs boson in gluon fusion, with or without an associated jet, as a benchmark process. The case of H +jet production is presented for the first time in an NLO+PS matched simulation. Uncertainties due to scale choices and non-perturbative effects are explored in the production of W^\pm and Z bosons in association with a jet. Corresponding results are compared to data from the Tevatron and LHC experiments.

1 Introduction

The central topic in the development of Monte-Carlo event generators during the past decade was the systematic inclusion of higher order QCD effects. One of the first approaches, the merging of leading-order (LO) multi-jet matrix elements of varying multiplicity with parton showers, has been pioneered and matured in a series of papers [1], such that by now it has become the accepted standard for simulating final states which include multi-jet topologies. It typically yields a very satisfactory description of experimental data, but due to the lack of virtual corrections it can never achieve the formal accuracy of a full next-to-leading order (NLO) calculation. This shortcoming is especially worrisome in the case of Standard Model Higgs-boson production through gluon fusion, where a large K -factor indicates substantial higher-order corrections, such that theoretical predictions should be made at next-to-leading order accuracy or better.

With the development of the MC@NLO [2] and POWHEG [3] techniques it became feasible to combine NLO accurate matrix-element calculations with parton showers. This technology is called NLO matching, in contrast to the LO merging described above. Ultimately, NLO matching techniques allow to carry out a full simulation of events, including hadronisation, hadron decays and the underlying event. While MC@NLO relies on a subtraction algorithm based on the parton shower approximation to collinear divergences in real-emission matrix elements, the POWHEG method effectively constructs a one-emission generator, similar

to a one-step parton shower, with evolution kernels determined by ratios of real-emission and Born matrix elements. In this respect the POWHEG method is very similar to traditional matrix-element correction techniques [4].

Despite having been proposed several years ago, the MC@NLO and POWHEG methods were not applied to processes with more than two external massless QCD particles until recently. This delay signals several complications which arise in reactions with additional light partons. Di-jet production [5] and $Z + j$ production [6] have now become available through the POWHEGBOX and predictions for W^\pm production in association with a bottom-antibottom pair have been made with both POWHEG [7] and MC@NLO [8]. Most recently, W^\pm plus two jets production was implemented [9].

In this publication the MC@NLO and POWHEG methods will be compared in some detail, and open issues related to their implementation and validation will be discussed. As benchmark processes, the production of Higgs-, W^\pm - and Z -bosons, alone or in association with one hard jet at Born level have been chosen. These processes are either signals central to the experimental program at the LHC, or they contribute as important backgrounds to many new physics searches [10]. Apart from that, QCD-associated W^\pm - and Z -production are of great interest, to study jet production and evolution in a hadron-collider environment at the energy frontier [11, 12], to improve the jet energy scale determination by the experiments, or to study multiple parton scattering processes. At the LHC as well as at the Tevatron, typically, good agreement is found when comparing respective data with merged leading-order predictions or with next-to-leading order perturbative QCD predictions, for instance from [13, 14]. This level of theoretical control and experimental precision suggests that the processes chosen here are indeed well-suited to serve as testbed for NLO matching methods.

The present paper is organised as follows: In Sec. 2 basic ideas underlying the MC@NLO and POWHEG strategies are reviewed. Similarities and differences between the two methods are discussed and potential pitfalls in their implementation are indicated. The solution to some of these problems is detailed in Sec. 3, where the MC@NLO algorithm is worked out in a formalism similar to [15]. This allows to elaborate on various aspects of the method regarding non-trivial colour and flavour configurations. Readers not interested in the technical details may skip this section. In Sec. 4 perturbative uncertainties related to scale variations and to the different exponentiation in the MC@NLO and POWHEG methods are highlighted. The impact of non-perturbative effects is investigated in Sec. 5 and results for W^\pm - and Z -production are compared to experimental data. Finally, Sec. 6 summarises the findings of this publication and outlines some possible extensions of the methods presented here.

2 Event generation with POWHEG and MC@NLO in a nutshell

This section is meant to highlight in a simple language the ideas of how NLO QCD calculations can be combined with subsequent parton showers. A common notation is established for POWHEG and MC@NLO and critical aspects related to the practical implementation for processes with non-trivial colour structure are discussed.

2.1 Anatomy of NLO calculations

In order to see how the existing matching algorithms work, consider first the structure of an NLO calculation. The total cross section can be written as

$$\sigma^{(\text{NLO})} = \int d\Phi_B \left[B(\Phi_B) + \tilde{V}(\Phi_B) + I^{(\text{S})}(\Phi_B) \right] + \int d\Phi_R \left[R(\Phi_R) - D^{(\text{S})}(\Phi_R) \right], \quad (2.1)$$

where $d\Phi_B$ and $d\Phi_R$ denote Born and real-emission phase space, respectively and B , \tilde{V} , $I^{(\text{S})}$, R and $D^{(\text{S})}$, are the matrix elements for the Born, virtual, integrated subtraction, real emission and real subtraction contribution. Note that for hadronic initial states \tilde{V} is defined such as to include the collinear mass-factorisation counterterms. All integrands include parton luminosity and flux factors. For simplicity it is assumed that the processes under consideration here have no identical QCD partons in the final state, a detailed discussion of symmetry factors is postponed to Sec. 3. In the subtraction formalisms most commonly employed to date [16, 17], subtraction terms can be written as the convolution of Born matrix elements with suitably

defined operators \tilde{K} , such that schematically

$$d\Phi_R D^{(S)}(\Phi_R) = d\Phi_B d\Phi_1 \left[B(\Phi_B) \otimes \tilde{K}(\Phi_1) \right] \quad \text{and} \quad I^{(S)}(\Phi_B) = \int d\Phi_1 \left[B(\Phi_B) \otimes \tilde{K}(\Phi_1) \right], \quad (2.2)$$

indicating that the two related contributions cancel locally in the Born phase space. This also suggests that the definition of the subtraction kernels \tilde{K} is somewhat arbitrary, as long as they exhibit the same singularity structure as the full real-emission matrix elements in the soft and collinear limits.

To combine an NLO calculation with a parton shower, it is essential to ensure that the result inherits the total cross section from the fixed-order calculation. This could trivially be achieved by multiplying a leading order plus parton shower simulation with a global K -factor - the ratio of NLO and LO cross section. The problem is that parton showers generate emissions which do not necessarily follow the pattern obtained from the real emission matrix elements, leading to a mismatch of radiation patterns at first order in the strong coupling constant α_s . In principle, this problem has been solved by the traditional matrix-element correction procedure outlined in [4], which is implemented for a number of processes in both HERWIG and PYTHIA. The essence of this method lies in the fact that, for the processes it is applied to, the product of Born-level contribution and parton shower evolution kernel K is larger than the corresponding real emission term R in the complete phase space of the extra emission. This allows to correct the first (hardest) emission with a factor $R/(BK)$, leading to the desired distribution in phase space. From this it can be seen that such an algorithm will fail for cases, where R is not always smaller than the Born-times-parton-shower result, or where the parton shower is not capable of filling the full phase space. In such cases a more detailed analysis is necessary.

2.2 Sudakov form factors

In this section the construction of the parton shower using Sudakov form factors will be briefly recalled. They are defined as

$$\Delta(t, t') = \exp \left\{ - \int_t^{t'} \frac{d\bar{t}}{\bar{t}} \int dz \int \frac{d\phi}{2\pi} J(\bar{t}, z, \phi) \frac{\alpha_s}{2\pi} K(\bar{t}, z, \phi) \right\} = \exp \left\{ - \int_t^{t'} d\Phi_1 \frac{\alpha_s}{2\pi} K(\Phi_1) \right\}, \quad (2.3)$$

where the sequence of emissions is ordered by a parameter t – typically related to the virtuality, transverse momentum or opening angle of the emission. Furthermore, z is the variable defining the splitting of energy or light-cone momentum of the two daughters emerging in the decay of the parton, and ϕ denotes the azimuthal angle. Collectively they define the one-emission phase space Φ_1 and its Jacobian J , while K is the splitting kernel encoding the detailed kinematical distribution due to soft-collinear enhancement and spin effects. For simplicity, parton luminosity factors are included into this kernel, and a detailed discussion is postponed to Sec. 3. Note that in all practical implementations of Eq. (2.3) the argument of the strong coupling is related to the transverse momentum of the splitting, given by the decay kinematics, i.e. by Φ_1 . For the sake of clarity this argument will be suppressed in this section.

This Sudakov form factor can be interpreted as a no-branching probability between the two scales t and t' . Obviously, $\{1 - \Delta(t, t')\}$ then yields the probability that a splitting has taken place in the interval between the two scales. Therefore, to first order in α_s , the cross section in the parton-shower approximation reads

$$\sigma_{PS}^{(LO)} = \int d\Phi_B B(\Phi_B) \left[\Delta(t_0, \mu_F^2) + \int_{t_0}^{\mu_F^2} d\Phi_1 \frac{\alpha_s}{2\pi} K(\Phi_1) \Delta(t, \mu_F^2) \right], \quad (2.4)$$

where t is determined by the kinematics of the first emission, $t = t(\Phi_1)$, such that it is smaller than the suitably chosen, process-dependent factorisation scale μ_F^2 , and where the arguments of the splitting kernel depend on this extra emission kinematics. The first term in the square bracket represents the probability of no extra emission to happen above the infrared cut-off t_0 of the parton shower, while the second term generates one emission above this scale. It can also be seen that the square bracket as a whole integrates to one, exposing the probabilistic nature of the parton shower, which leaves the total cross section of an event sample unchanged.

2.3 Matrix element corrections and POWHEG

Applying matrix element corrections to the parton shower transforms the equation above, Eq. (2.4), into

$$\sigma_{\text{MEC}}^{(\text{LO})} = \int d\Phi_B B(\Phi_B) \left[\bar{\Delta}(t_0, \mu_F^2) + \int_{t_0}^{\mu_F^2} d\Phi_1 \frac{R(\Phi_B, \Phi_1)}{B(\Phi_B)} \bar{\Delta}(t, \mu_F^2) \right], \quad (2.5)$$

where the modified Sudakov form factor $\bar{\Delta}$ reads

$$\bar{\Delta}(t, t') = \exp \left\{ - \int_t^{t'} d\Phi_1 \frac{R(\Phi_B, \Phi_1)}{B(\Phi_B)} \right\}. \quad (2.6)$$

Again, the square bracket in Eq. (2.5) integrates to one, and the cross section of an event sample is identical to the Born cross section. However, the distribution of the first (hardest) emission, to first order in α_s will follow the pattern given by the full real emission matrix element, and is thus correct to $\mathcal{O}(\alpha_s)$.

In order to achieve full $\mathcal{O}(\alpha_s)$ -accuracy in both the cross section of the produced event sample and the pattern of the first emission it is mandatory to replace the differential Born cross section $d\Phi_B B$ with an expression that integrates to the full NLO cross section of Eq. (2.1). This is achieved by the substitution

$$B(\Phi_B) \longrightarrow \bar{B}(\Phi_B) = B(\Phi_B) + \tilde{V}(\Phi_B) + I^{(\text{S})}(\Phi_B) + \int d\Phi_1 \left[R(\Phi_B, \Phi_1) - D^{(\text{S})}(\Phi_B, \Phi_1) \right]. \quad (2.7)$$

It is straightforward to interpret this term as an NLO-weighted Born-level cross section, or, put in a slightly different way, a Born-level cross section that is augmented with a *local K-factor*.

Equipped with this definition the expression for the cross section in the POWHEG-formalism reads

$$\sigma_{\text{POWHEG}}^{(\text{NLO})} = \int d\Phi_B \bar{B}(\Phi_B) \left[\bar{\Delta}(t_0) + \int_{t_0}^{\mu_F^2} d\Phi_1 \frac{R(\Phi_B, \Phi_1)}{B(\Phi_B)} \bar{\Delta}(t) \right]. \quad (2.8)$$

This expression is indeed accurate up to the first order in the strong coupling constant for *both* the total cross section of the event sample and the differential cross section with respect to the kinematics of the first emission.

2.4 Modified subtraction and MC@NLO

Taking a closer look at the master formula of the POWHEG-approach, Eq. (2.8), reveals a potential problem: There are real-emission contributions which cannot be obtained from a Born-level configuration by simply emitting an extra parton. Examples for this include flavour configurations such as $u\bar{u} \rightarrow c\bar{s}e^-\bar{\nu}_e$ or kinematical configurations such as radiation zeroes [18]. In this context it is important to note that infrared singular structures in the NLO part of the calculation – i.e. in the virtual and real terms – can always be traced back to the soft or collinear emission off an underlying Born configuration. Therefore, it is well motivated to split the real-emission matrix elements R into an infrared-singular (soft) and an infrared-regular (hard) part, $D^{(\text{A})}$ and $H^{(\text{A})}$, respectively: $R = D^{(\text{A})} + H^{(\text{A})}$ [19]. Equation (2.1) then transforms into

$$\begin{aligned} \sigma^{(\text{NLO})} = & \int d\Phi_B \left[B(\Phi_B) + \tilde{V}(\Phi_B) + I^{(\text{S})}(\Phi_B) \right] \\ & + \int d\Phi_R \left[D^{(\text{A})}(\Phi_R) - D^{(\text{S})}(\Phi_R) \right] + \int d\Phi_R H^{(\text{A})}(\Phi_R), \end{aligned} \quad (2.9)$$

and the cross section in the POWHEG formalism, Eq. (2.8), can be rewritten as

$$\sigma_{\text{POWHEG}}^{(\text{NLO})} = \int d\Phi_B \bar{B}^{(\text{A})}(\Phi_B) \left[\bar{\Delta}^{(\text{A})}(t_0) + \int_{t_0}^{\mu_F^2} d\Phi_1 \frac{D^{(\text{A})}(\Phi_B, \Phi_1)}{B(\Phi_B)} \bar{\Delta}^{(\text{A})}(t) \right] + \int d\Phi_R H^{(\text{A})}(\Phi_R), \quad (2.10)$$

where

$$\bar{B}^{(\text{A})}(\Phi_B) = B(\Phi_B) + \tilde{V}(\Phi_B) + I^{(\text{S})}(\Phi_B) + \int d\Phi_1 \left[D^{(\text{A})}(\Phi_B, \Phi_1) - D^{(\text{S})}(\Phi_B, \Phi_1) \right] \quad (2.11)$$

and, with obvious notation,

$$\bar{\Delta}^{(A)}(t, t') = \exp \left\{ - \int_t^{t'} d\Phi_1 \frac{D^{(A)}(\Phi_B, \Phi_1)}{B(\Phi_B)} \right\}. \quad (2.12)$$

In this manner, the non-singular contributions at real-emission level are correctly captured in the POWHEG approach and the exponentiation of non-singular terms is avoided to some extent.

One can now define $D^{(A)} = D^{(S)}$, leading to a tremendous simplification of Eq. (2.11). Additionally, for the subtraction kernels \tilde{K} one can use the parton shower splitting kernels K . This in fact is how the MC@NLO formalism works, which can be understood as a special case of the generalised POWHEG method. Specified for MC@NLO, Eq. (2.10) reads

$$\sigma_{\text{MC@NLO}}^{(\text{NLO})} = \int d\Phi_B \bar{B}^{(\text{BK})}(\Phi_B) \left[\Delta(t_0) + \int_{t_0} d\Phi_1 \frac{\alpha_s}{2\pi} K(\Phi_1) \Delta(t) \right] + \int d\Phi_R H^{(\text{BK})}(\Phi_B), \quad (2.13)$$

where the modified Born contribution and the regular real-emission part are defined as

$$\begin{aligned} \bar{B}^{(\text{BK})}(\Phi_B) &= B(\Phi_B) + \tilde{V}(\Phi_B) + \int d\Phi_1 \left[B(\Phi_B) K(\Phi_1) \right] \\ H^{(\text{BK})}(\Phi_R) &= R(\Phi_R) - [\text{BK}] (\Phi_R). \end{aligned} \quad (2.14)$$

Note, that when using the parton shower kernels to define subtraction terms their convolution with the Born matrix element reverts to a simple product, describing only the collinear singularities. Thus, this definition is usually correct to leading colour only. Care must be taken in processes involving more than three partons in order to cancel soft divergences in real-emission matrix elements. These problems will be addressed in Sec. 3.4.

2.5 Subtleties in practical implementations of POWHEG and MC@NLO

At the level of detail of the discussion up to now, an implementation of both methods, POWHEG and MC@NLO, seems quite straightforward. However, there are a number of subtleties, which have not been presented yet in a coherent fashion in a journal publication. Some of them will be dealt with in Sec. 3.

1. Linking R and B in POWHEG

The real-emission contribution R must be linked to the underlying Born configuration B in a meaningful way in both the \bar{B} term and the hardest emission kernel R/B of the POWHEG master formula, Eq. (2.8). This means that a momentum map needs to be found, linking Φ_R and Φ_B and covering the full phase space, possibly also including helicity and colour. Such a map is conveniently defined by the infrared subtraction method. For the case of Catani-Seymour (CS) subtraction [16] various dipole terms will then automatically lead to various Born-level configurations for the same real-emission term, which is problematic for a numerically stable integration in Eq. (2.7) as the cancellation of soft divergences requires more than one contribution. This problem may be significantly alleviated using Frixione-Kunszt-Signer (FKS) subtraction [17], but will be ignored in the context of this publication, as the focus lies on the MC@NLO method.

2. Subtraction of infrared divergent sub-leading colour terms in MC@NLO

The problem of soft divergences outlined above has yet another manifestation, this time in the MC@NLO algorithm. To see the origin of this, note that the parton shower is based on a leading logarithmic and leading colour approximation. Using it, without modification, to construct subtraction terms will therefore necessarily miss divergences in sub-leading colour configurations. This presents a clear obstacle to apply the method to processes where infrared divergences in such sub-leading colour configurations emerge. In [20], and referring to ideas outlined in the original MC@NLO publication [2], this problem was overcome for the case of heavy flavour hadro-production processes of the type $gg \rightarrow Q\bar{Q}$ and $q\bar{q} \rightarrow Q\bar{Q}$ at Born-level. An additional factor was introduced there, which multiplies the emission probability of soft partons, since the soft singularity structure cannot be associated with the soft divergence of an Altarelli-Parisi splitting function [20]. In fact, the same method is applied in the case of the recently presented aMC@NLO [8, 21]. Although it is possibly hard to prove that such a solution works in a process-independent way, up to now no dependence of physical results on the choice of this soft function has been reported.

3. Choice of scales in POWHEG and MC@NLO

It was argued in [3], based on [22], that the proper choice of scale for the strong coupling in the kernel R/B of the POWHEG Sudakov form factor is given by the transverse momentum of the emission generated in the branching process. Similarly, it was pointed out in [2] that the scale in the evolution kernel of an MC@NLO should be the transverse momentum. This particular choice of scale effectively resums a certain class of universal higher-order corrections. It typically leads to a very good agreement between the results from existing parton shower algorithms and experimental data and is therefore employed in all standard Monte-Carlo event generators [23].

Such a scale choice ultimately implies higher-order corrections to the event kinematics. The key point is that the differential NLO cross section defined by Eq. (2.7) can be evaluated with arbitrary scales. However, the functional form of the scale must be infrared and collinear safe. This is not the case for the transverse momentum in the branching process, because, in contrast to the Sudakov branching algorithm, there is no infrared cutoff in the calculation of \bar{B} . Thus, the first-order expansion of the Sudakov form factor does not reproduce the exact same real-correction / subtraction terms as the NLO calculation, leading to a misbinning effect, which can be numerically large in the logarithmically enhanced regions of phase space. In this publication the problem is only noted, and no proper general solution is proposed.

4. Exponentiation of non-leading terms in POWHEG and MC@NLO

Ultimately, there is a last subtlety, which has also been discussed in [24], summarising some previous work by the same authors. It is related to the form of the Sudakov form factor and the phase space available for the hardest emission. The evolution kernel R/B in the POWHEG method clearly includes terms beyond leading logarithms and it is somewhat questionable in how far they should be exponentiated. The difference compared to evolution kernels in the parton shower may lead to sizable effects, up to orders of magnitude, when results for the hard, non-logarithmic tails of distributions in the POWHEG approach are compared with those of the pure NLO calculation, see for instance [25, 7]. In the case of the POWHEGBOX and processes implemented therein, the authors use a tunable function in order to eliminate unwanted hard tails stemming from this exponentiation problem.

Interestingly enough, a similar problem, with a different origin, can be encountered in the MC@NLO formalism. There, the Sudakov form factor has kernels which reduce to Altarelli-Parisi splitting functions in the collinear and soft-collinear limits. However, away from these limits, additional terms may emerge, which do have a sizable, and in principle uncontrollable impact. In the implementation presented here, based on CS subtraction [26] and a parton shower built on CS subtraction kernels [27] this leads to similarly hard tails in some distributions. Note that the starting scales of the parton shower are maximised for the first emission, in order to fill the full phase space, similar to a power-shower approach [28]. The effect of this seems to become more severe for more exclusive processes, i.e. for processes with additional jets in the final state, which in the parton shower picture would provide additional constraints on the phase space available for further emissions. In the implementation here, a phase-space constraint has been added to the subtraction explicitly, hence limiting the logarithmically enhanced region of the real-emission contribution and adding the hard regions to the regular contribution. The impact of the choice of this constraint is analysed quantitatively in Sec. 4, and some recommendations for the specific values are made. Here, the respective uncertainties are referred to as “exponentiation uncertainties”.

It is worth noting that in both cases, POWHEG and MC@NLO, the problem manifests itself in those regions of phase space, which are not logarithmically enhanced, and where naturally any parton shower approximation breaks down. By constraining the phase space in a controlled way this issue can be resolved; and in fact it clearly is mandatory to solve it in order to formally prove the correctness of any multi-jet merging algorithm at next-to leading order ¹.

3 POWHEG and MC@NLO in detail

When combining next-to-leading order matrix elements with parton showers, the logarithmic corrections encoded in the Sudakov form factor must be matched to the full next-to-leading order prediction of the parton-level calculation. This is usually achieved either by subtracting the first-order expansion of the

¹ This is a point that was obviously missed or ignored by the authors of [29].

resummed result from the NLO calculation (MC@NLO), or by exponentiating the full real-emission correction in the resummation (POWHEG). One can also construct mixed schemes, as argued in Sec. 2.4. The difference which is induced by the exponentiation of subleading corrections vanishes for soft or collinear parton emission. However, it might play an important role in other regions of the phase space. In the following, a formalism that allows to discuss the difference between the MC@NLO and POWHEG methods in more detail is reviewed.

3.1 Notation and definitions

Denoting sets of n particles in a $2 \rightarrow (n-2)$ process by $\{\vec{a}\} = \{a_1, \dots, a_n\}$, while their respective flavours and momenta are specified separately through $\{\vec{f}\} = \{f_1, \dots, f_n\}$ and $\{\vec{p}\} = \{p_1, \dots, p_n\}$, the generic expression for a fully differential Born-level cross section can be written as a sum over all contributing flavour configurations:

$$d\sigma_B(\{\vec{p}\}) = \sum_{\{\vec{f}\}} d\sigma_B(\{\vec{a}\}) , \quad \text{where} \quad d\sigma_B(\{\vec{a}\}) = d\Phi_B(\{\vec{p}\}) \mathcal{B}(\{\vec{a}\}) , \quad (3.1)$$

The individual terms in the sum are given by

$$\begin{aligned} \mathcal{B}(\{\vec{a}\}) &= \mathcal{L}(\{\vec{a}\}) \mathcal{B}(\{\vec{a}\}) , & \mathcal{B}(\{\vec{a}\}) &= \frac{1}{F(\{\vec{p}\})} \frac{1}{S(\{\vec{f}\})} |\mathcal{M}_B|^2(\{\vec{a}\}) , \\ d\Phi_B(\{\vec{p}\}) &= \frac{dx_1}{x_1} \frac{dx_2}{x_2} d\Phi_B(\{\vec{p}\}) , & \mathcal{L}(\{\vec{a}\}; \mu^2) &= x_1 f_{f_1}(x_1, \mu^2) x_2 f_{f_2}(x_2, \mu^2) , \end{aligned} \quad (3.2)$$

where $|\mathcal{M}_B|^2(\{\vec{a}\})$ denotes the partonic matrix element squared, $d\Phi_B(\{\vec{p}\})$ is the corresponding differential n -particle partonic phase-space element, $S(\{\vec{f}\})$ is the symmetry factor, $F(\{\vec{p}\})$ is the flux factor, and \mathcal{L} is the parton luminosity².

In a similar fashion, the real-emission part of the QCD next-to-leading order cross section can be written as a sum, depending on parton configurations $\{a_1, \dots, a_{n+1}\}$, by replacing the Born-level matrix elements \mathcal{B} with the real-emission matrix elements \mathcal{R} and the Born-level phase space $d\Phi_B$ with the real-emission phase-space $d\Phi_R$.

It is then useful to introduce a notation for mappings from real-emission parton configurations to Born-level parton configurations and vice versa. They are given by (cf. [15])

$$b_{ij,k}(\{\vec{a}\}) = \left\{ \begin{array}{l} \{\vec{f}\} \setminus \{f_i, f_j\} \cup \{f_{i\tilde{j}}\} \\ \{\vec{p}\} \rightarrow \{\vec{p}\} \end{array} \right\} \quad \text{and} \quad r_{\tilde{i}\tilde{j},\tilde{k}}(f_i, \Phi_{R|B}^{ij,k}; \{\vec{a}\}) = \left\{ \begin{array}{l} \{\vec{f}\} \setminus \{f_{i\tilde{j}}\} \cup \{f_i, f_j\} \\ \{\vec{p}\} \rightarrow \{\vec{p}\} \end{array} \right\} . \quad (3.3)$$

The map $b_{ij,k}(a)$ combines the partons a_i and a_j into a common “mother” parton $a_{i\tilde{j}}$, in the presence of the spectator a_k by defining a new flavour $f_{i\tilde{j}}$ and by redefining the particle momenta. The inverse map, $r_{\tilde{i}\tilde{j},\tilde{k}}(a)$ determines the parton configuration of a real-emission subprocess from a Born parton configuration and a related branching process $\tilde{i}\tilde{j}, \tilde{k} \rightarrow ij, k$. The radiative variables $\Phi_{R|B}^{ij,k}$, denoted Φ_1 in Sec. 2 for brevity, are thereby employed to turn the n -parton momentum configuration into an $(n+1)$ -parton momentum configuration.

The real-emission matrix elements, $\mathcal{R}(\{\vec{a}\})$, can be approximated in the soft and collinear limits by subtraction terms $\mathcal{D}_{ij,k}^{(S)}(\{\vec{a}\})$, which capture the universal singularity structure when two partons i and j become collinear, or one of them becomes soft in the presence of a spectator parton k .

$$\mathcal{R} \xrightarrow{i,j \text{ collinear} \atop i,j \text{ soft}} \mathcal{D}_{ij,k}^{(S)}(\{\vec{a}\}) . \quad (3.4)$$

These subtraction terms are related to the ones defined in Sec. 2 through $\mathcal{D}^{(S)} \rightarrow \mathcal{L}(\{\vec{a}\}) \mathcal{D}_{ij,k}^{(S)}(\{\vec{a}\})$, with implicit notation of dipole indices, phase space and flavour configuration on the left hand side. They are not uniquely defined, but can be constructed, for example, using the Catani-Seymour method [16] or the

² In the case of leptonic initial states, and ignoring QED initial-state radiation, the parton distribution functions $f(x, \mu^2)$ are replaced by $\delta(1-x)$.

FKS approach [17]. Furthermore they can be restricted in phase space or extended with an arbitrary finite function [26]. Similar terms can also be computed in a parton-shower approximation as

$$\mathcal{R}^{ij \text{ collinear}} \mathcal{D}_{ij,k}^{(\text{PS})}(\{\vec{a}\}) = \mathcal{B}(b_{ij,k}(\{\vec{a}\})) \frac{S(b_{ij,k}(\{\vec{f}\}))}{S(\{\vec{f}\})} \frac{1}{2p_i p_j} 8\pi \alpha_s \mathcal{K}_{ij,k}(p_i, p_j, p_k), \quad (3.5)$$

where $\mathcal{K}_{ij,k}$ denote the parton-shower evolution kernels. These approximate subtraction terms are identified with the ones in Eq. (2.14) as $\text{BK} \rightarrow \mathcal{L}(\{\vec{a}\}) \mathcal{D}_{ij,k}^{(\text{PS})}(\{\vec{a}\})$, again with implicit notation of dipole indices, flavour and momentum configuration on the left hand side. The parton-shower approximation is meaningful only in the collinear region, as it implements an exact factorisation of the colour structure into a Born part and an emission part. In many cases also a factorisation of the helicity structure is assumed.

3.2 From fixed-order to resummation

Section 2 only introduced expressions for the *total cross section* in the MC@NLO and POWHEG methods. A detailed discussion requires an analysis of the expectation value of arbitrary infra-red safe observables. The respective formulae are developed in the following.

Using the subtraction terms introduced in Eq. (3.4), the expectation value of an observable O is determined to next-to-leading order accuracy as

$$\begin{aligned} \langle O \rangle^{(\text{NLO})} = & \sum_{\{\vec{f}\}} \int d\Phi_B(\{\vec{p}\}) \left[\mathcal{B}(\{\vec{a}\}) + \tilde{\mathcal{V}}(\{\vec{a}\}) + \sum_{\{\tilde{i}, \tilde{k}\}} \mathcal{I}_{\tilde{i}, \tilde{k}}^{(\text{S})}(\{\vec{a}\}) \right] O(\{\vec{p}\}) \\ & + \sum_{\{\vec{f}\}} \int d\Phi_R(\{\vec{p}\}) \left[\mathcal{R}(\{\vec{a}\}) O(\{\vec{p}\}) - \sum_{\{ij,k\}} \mathcal{D}_{ij,k}^{(\text{S})}(\{\vec{a}\}) O(b_{ij,k}(\{\vec{p}\})) \right]. \end{aligned} \quad (3.6)$$

where $\mathcal{I}^{(\text{S})}(\{\vec{a}\})$ represent the subtraction terms $\mathcal{D}^{(\text{S})}(\{\vec{a}\})$ integrated over the extra-emission phase space. Note that the configurations $\{\vec{f}\}$, $\{\vec{p}\}$ and $\{\vec{a}\}$ on the second line each include one more particle.

This equation can be modified by adding and subtracting an additional arbitrary set of subtraction terms $\mathcal{D}^{(\text{A})}(\{\vec{a}\})$ with the same kinematics mapping as $\mathcal{D}^{(\text{S})}(\{\vec{a}\})$

$$\begin{aligned} \langle O \rangle^{(\text{NLO})} = & \sum_{\{\vec{f}\}} \int d\Phi_B(\{\vec{p}\}) \bar{\mathcal{B}}^{(\text{A})}(\{\vec{p}\}) O(\{\vec{p}\}) \\ & + \sum_{\{\vec{f}\}} \int d\Phi_R(\{\vec{p}\}) \left[\mathcal{R}(\{\vec{a}\}) O(\{\vec{p}\}) - \sum_{\{ij,k\}} \mathcal{D}_{ij,k}^{(\text{A})}(\{\vec{a}\}) O(b_{ij,k}(\{\vec{p}\})) \right], \end{aligned} \quad (3.7)$$

where the function $\bar{\mathcal{B}}^{(\text{A})}(\{\vec{a}\})$ is defined as

$$\begin{aligned} \bar{\mathcal{B}}^{(\text{A})}(\{\vec{a}\}) = & \mathcal{B}(\{\vec{a}\}) + \tilde{\mathcal{V}}(\{\vec{a}\}) + \sum_{\{\tilde{i}, \tilde{k}\}} \mathcal{I}_{\tilde{i}, \tilde{k}}^{(\text{S})}(\{\vec{a}\}) \\ & + \sum_{\{\tilde{i}, \tilde{j}, \tilde{k}\}} \sum_{f_i=q,g} \int d\Phi_{R|B}^{ij,k} \left[\mathcal{D}_{ij,k}^{(\text{A})}(r_{\tilde{i}, \tilde{j}, \tilde{k}}(\{\vec{a}\})) - \mathcal{D}_{ij,k}^{(\text{S})}(r_{\tilde{i}, \tilde{j}, \tilde{k}}(\{\vec{a}\})) \right], \end{aligned} \quad (3.8)$$

and where $d\Phi_{R|B}^{ij,k}$ represents an integral over the radiative phase space.

When combining fixed-order calculations with resummation, the task is to define a unique starting condition for the parton shower. As was argued in [2], it is not possible to process the terms $\mathcal{R}(\{\vec{a}\})$ and $\mathcal{D}_{ij,k}^{(\text{A})}(\{\vec{a}\})$ in Eq. (3.7) separately because this would lead to double-counting. Instead, the problem is solved if the observables on the second line of Eq. (3.7) are both assumed to depend on the momentum configuration $\{\vec{p}\}$.

This leads to

$$\begin{aligned} \langle O \rangle^{(\text{NLO})} = & \sum_{\{\vec{f}\}} \int d\Phi_B(\{\vec{p}\}) \bar{B}^{(A)}(\{\vec{p}\}) O(\{\vec{p}\}) \\ & + \sum_{\{\vec{f}\}} \int d\Phi_R(\{\vec{p}\}) \left[R(\{\vec{a}\}) - \sum_{\{ij,k\}} D_{ij,k}^{(A)}(\{\vec{a}\}) \right] O(\{\vec{p}\}) + \langle O \rangle^{(\text{corr})}, \end{aligned} \quad (3.9)$$

introducing the correction term ³

$$\langle O \rangle^{(\text{corr})} = \sum_{\{\vec{f}\}} \int d\Phi_R(\{\vec{p}\}) \sum_{\{ij,k\}} D_{ij,k}^{(A)}(\{\vec{a}\}) \left[O(\{\vec{p}\}) - O(b_{ij,k}(\{\vec{p}\})) \right]. \quad (3.10)$$

The essence of both the MC@NLO and POWHEG methods is to generate Eq. (3.10) by using a Sudakov branching algorithm, which is formulated in terms of an evolution variable t , where $t \propto 2p_i p_j$. Let a corresponding form factor be defined as

$$\bar{\Delta}^{(A)}(t; \{\vec{a}\}) = \prod_{\{\tilde{ij}, \tilde{k}\}} \bar{\Delta}_{\tilde{ij}, \tilde{k}}^{(A)}(t; \{\vec{a}\}), \quad (3.11)$$

where

$$\begin{aligned} \bar{\Delta}_{\tilde{ij}, \tilde{k}}^{(A)}(t; \{\vec{a}\}) = & \exp \left\{ - \sum_{f_i=q,g} \int d\Phi_{R|B}^{ij,k} \Theta(t(\Phi_{R|B}^{ij,k}) - t) \right. \\ & \times \left. \frac{1}{S_{ij}} \frac{S(r_{\tilde{ij}, \tilde{k}}(f_i; \{\vec{f}\}))}{S(\{\vec{f}\})} \frac{D_{ij,k}^{(A)}(r_{\tilde{ij}, \tilde{k}}(f_i, \Phi_{R|B}^{ij,k}; \{\vec{a}\}))}{B(\{\vec{a}\})} \right\}. \end{aligned} \quad (3.12)$$

The ratio of symmetry factors, including S_{ij} , is explained in detail in [15]. It accounts for the way in which the phase space is successively filled by a parton shower.

It can then be proven [2, 3, 15], that the following formula for the expectation value of an infrared safe observable reproduces Eq. (3.9) to $\mathcal{O}(\alpha_s)$:

$$\begin{aligned} \langle O \rangle^{(\text{NLOMC})} = & \sum_{\{\vec{f}\}} \int d\Phi_B(\{\vec{p}\}) \bar{B}^{(A)}(\{\vec{a}\}) \left[\underbrace{\bar{\Delta}^{(A)}(t_0; \{\vec{a}\})}_{\text{unresolved}} O(\{\vec{p}\}) \right. \\ & + \sum_{\{\tilde{ij}, \tilde{k}\}} \sum_{f_i=q,g} \int d\Phi_{R|B}^{ij,k} \Theta(t(\Phi_{R|B}^{ij,k}) - t_0) O(r_{\tilde{ij}, \tilde{k}}(\{\vec{p}\})) \\ & \times \underbrace{\frac{1}{S_{ij}} \frac{S(r_{\tilde{ij}, \tilde{k}}(f_i; \{\vec{f}\}))}{S(\{\vec{f}\})} \frac{D_{ij,k}^{(A)}(r_{\tilde{ij}, \tilde{k}}(f_i, \Phi_{R|B}^{ij,k}; \{\vec{a}\}))}{B(\{\vec{a}\})} \bar{\Delta}^{(A)}(t; \{\vec{a}\})}_{\text{resolved, singular}} \left. \right] \\ & + \sum_{\{\vec{f}\}} \int d\Phi_R(\{\vec{p}\}) \left[\underbrace{R(\{\vec{a}\}) - \sum_{ij,k} D_{ij,k}^{(A)}(\{\vec{a}\})}_{\text{resolved, non-singular}} O(\{\vec{p}\}) \right]. \end{aligned} \quad (3.13)$$

NLO Monte-Carlo events reproducing Eq. (3.13) can be generated in the following way:

- A seed event is produced according to either the first or the second line of Eq. (3.9), not including the correction factor $\langle O \rangle^{(\text{corr})}$.

³ The dependence of the observable O on the kinematics of the partonic final state makes the need for a correction term $\langle O \rangle^{(\text{corr})}$ manifest. This term integrates to zero in Eq. (2.9), as $O=1$ and the phase-space dependence is trivial.

- If the second line is chosen (\mathbb{H} -event) the event has real-emission kinematics and is kept as-is. This generates the “resolved, non-singular” term of Eq. (3.13)
- If the first line is chosen (\mathbb{S} -event), the event has Born-like kinematics and is processed through a one-step Sudakov branching algorithm described by Eqs. (3.11) and (3.12). The necessary techniques for that case will be detailed in Sec. 3.4. An emission might or might not occur, which is represented by the “resolved, singular” and “unresolved” terms of Eq. (3.13), respectively.

3.3 Explicit construction of POWHEG and MC@NLO

Equation (3.13) becomes particularly simple when

$$D_{ij,k}^{(A)} \rightarrow D_{ij,k}^{(S)}. \quad (3.14)$$

In this special case the integral over the radiative phase space in Eq. (3.8) is zero. This is the essence of the MC@NLO technique. It can be thought of as a method which uses the Sudakov branching probability (e.g. a parton-shower approximation of real-emission matrix elements, similar to Eq. (3.5)) for subtraction. This crude interpretation will be refined in Sec. 3.4.

The POWHEG method, in its original form, on the other hand, defines

$$D_{ij,k}^{(A)} \rightarrow \rho_{ij,k}(\{\vec{a}\}) R(\{\vec{a}\}) \quad \text{where} \quad \rho_{ij,k}(\{\vec{a}\}) = \frac{\mathcal{D}_{ij,k}^{(S)}(\{\vec{a}\})}{\sum_{mn,l} \mathcal{D}_{mn,l}^{(S)}(\{\vec{a}\})}, \quad (3.15)$$

leading to a vanishing \mathbb{H} -term. The POWHEG method can be thought of as exponentiating the full radiative corrections into a Sudakov form factor. As such, it bears strong similarity to matrix-element corrected parton showers. This aspect has been discussed extensively in [15, 30].

One can construct a mixed scheme, where $D_{ij,k}^{(A)}$ is defined as

$$D_{ij,k}^{(A)} \rightarrow \rho_{ij,k}(\{\vec{a}\}) \left[R(\{\vec{a}\}) - R^{(r)}(\{\vec{a}\}) \right], \quad (3.16)$$

with $R^{(r)}$ an arbitrary infrared-finite part of the real-emission cross section and $\rho_{ij,k}$ given by Eq. (3.15). This method was originally proposed in [19] to deal with the problem of radiation zeros in the W^\pm -production process. It allows to interpolate smoothly between the original POWHEG strategy and the MC@NLO method.

Note that all the above choices of $D_{ij,k}^{(A)}$ fulfil the requirement that the kinematics and flavour mapping be identical to the one in $D_{ij,k}^{(S)}$, cf. Eq. (3.7).

3.4 Event-generation techniques

In the parton-shower approximation, Eq. (3.12) would read

$$\Delta_{\vec{ij},\vec{k}}(t', t''; \{\vec{a}\}) = \exp \left\{ - \sum_{f_i=q,g} \int_{t'}^{t''} \frac{dt}{t} \int_{z_{\min}}^{z_{\max}} dz \int_0^{2\pi} \frac{d\phi}{2\pi} J_{ij,k}(t, z, \phi) \right. \\ \left. \times \frac{1}{S_{ij}} \frac{\alpha_s}{2\pi} \mathcal{K}_{ij,k}(t, z, \phi) \frac{\mathcal{L}(r_{\vec{ij},\vec{k}}(f_i, t, z, \phi; \{\vec{a}\}); t)}{\mathcal{L}(\{\vec{a}\}; t)} \right\}, \quad (3.17)$$

where z is called the splitting variable of the parton-shower model and $J_{ij,k}$ is the Jacobian factor associated with the transformation of $d\Phi_{R|B}^{ij,k}$ into $dt dz d\phi$ [15].

It is well known how to generate emissions according to Eq. (3.17). The task of a proper implementation of MC@NLO and POWHEG is, however, to employ Eq. (3.12). This can involve subtraction terms which are negative, due to subleading colour configurations in the real-emission matrix elements, cf. Sec. 2.5. Exponentiating these terms leads to a form factor larger than one, which cannot be interpreted in terms of a no-branching probability.

In order to be able to still generate these form factors in a Markov chain Monte Carlo, a technique for weighted parton showers can be employed, which was outlined in [31] and reformulated in [32]. As it needs

to be modified slightly in the current context, it is briefly discussed here again. The method is based on an extension of the veto algorithm [33]. When incorporating an analytic weight into this algorithm one must account for both, modified acceptance and rejection probabilities.

Let t be the parton-shower evolution variable and $f(t)$ the splitting kernel \mathcal{K} , integrated over the splitting variable z .⁴ The differential probability for generating a branching at scale t , when starting from an upper evolution scale t' is then given by

$$\mathcal{P}(t, t') = f(t) \exp \left\{ - \int_t^{t'} d\bar{t} f(\bar{t}) \right\}. \quad (3.18)$$

A new scale t is therefore found as

$$t = F^{-1} [F(t') + \log \#] \quad \text{where} \quad F(t) = \int_t d\bar{t} f(\bar{t}), \quad (3.19)$$

and where $\#$ is a random number between zero and one. The key point of the veto algorithm is, that even if the integral $F(t)$ is unknown, one can still generate events according to \mathcal{P} using an overestimate $g(t) \geq f(t)$ with a known integral $G(t)$. Firstly, a value t is generated as $t = G^{-1} [G(t') + \log \#]$. Secondly, the value is accepted with probability $f(t)/g(t)$. A splitting at t with n intermediate rejections is then produced with probability

$$\begin{aligned} \mathcal{P}_n(t, t') &= \frac{f(t)}{g(t)} g(t) \exp \left\{ - \int_t^{t_1} d\bar{t} g(\bar{t}) \right\} \\ &\times \prod_{i=1}^n \left[\int_{t_{i-1}}^{t_{i+1}} dt_i \left(1 - \frac{f(t_i)}{g(t_i)} \right) g(t_i) \exp \left\{ - \int_{t_i}^{t_{i+1}} d\bar{t} g(\bar{t}) \right\} \right], \end{aligned} \quad (3.20)$$

where $t_{n+1} = t'$ and $t_0 = t$. The nested integrals in Eq. (3.20) can be disentangled, and summing over n leads to the exponentiation of the factor $g(t) - f(t)$, such that Eq. (3.18) is reproduced [33].

The purpose here is to introduce an additional overestimate $h(t)$. The additional weight $g(t)/h(t)$ is then applied analytically rather than using a hit-or-miss method. This leads to the following expression for the differential probability to generate an emission at t with n rejections between t and t'

$$\begin{aligned} \mathcal{P}_n(t, t') &= \frac{f(t)}{g(t)} h(t) \exp \left\{ - \int_t^{t_1} d\bar{t} h(\bar{t}) \right\} \\ &\times \prod_{i=1}^n \left[\int_{t_{i-1}}^{t_{i+1}} dt_i \left(1 - \frac{f(t_i)}{g(t_i)} \right) h(t_i) \exp \left\{ - \int_{t_i}^{t_{i+1}} d\bar{t} h(\bar{t}) \right\} \right]. \end{aligned} \quad (3.21)$$

In order to recover the desired distribution, the following analytic weight needs to be applied

$$w(t, t_1, \dots, t_n) = \frac{g(t)}{h(t)} \prod_{i=1}^n \frac{g(t_i)}{h(t_i)} \frac{h(t_i) - f(t_i)}{g(t_i) - f(t_i)}. \quad (3.22)$$

Here the term $g(t)/h(t)$ is due to the acceptance of the emission. The product, which is needed for an exponentiation of $h(t) - f(t)$ instead of $g(t) - f(t)$, runs over all correction weights for rejected steps.

In the remainder of this paper, the functions f , g and h are chosen as follows:

$$f \rightarrow D^{(A)}, \quad g \rightarrow C f, \quad \text{and} \quad h \rightarrow D^{(PS)}, \quad (3.23)$$

where $C \approx 2$ is a constant.

4 Analysis of perturbative uncertainties

In the following the uncertainties discussed in Sec. 2.5 are investigated in detail. The event generator SHERPA [34] sets the framework for this study, including its automated MC@NLO implementation, the

⁴ For simplicity, the existence of only one splitting function is assumed, i.e. that there is no flavour change of the splitter during the evolution. The extension to flavour changing splittings is straightforward, but it would unnecessarily complicate the notation at this point.

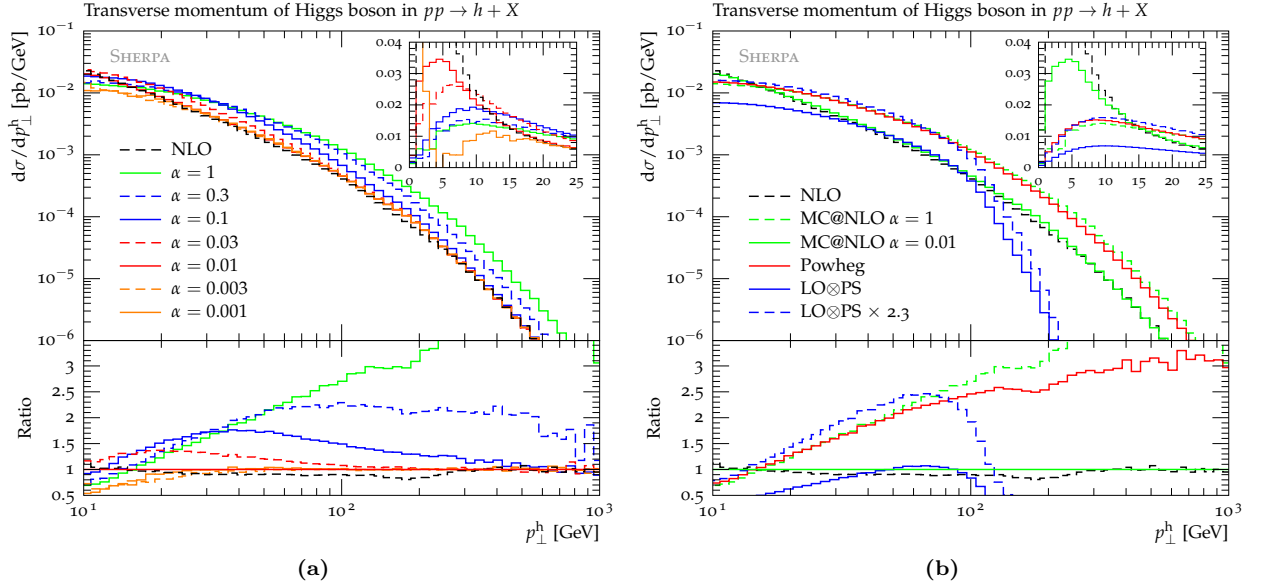


Figure 1: Transverse momentum of the Higgs boson in inclusive Higgs boson production ($m_h = 120$ GeV) at $E_{\text{cms}} = 7$ TeV. The variation of MC@NLO predictions with varying α_{cut} (denoted α in the legend) is shown in Fig. (a), while Fig. (b) compares the MC@NLO, POWHEG and LO \otimes PS methods.

matrix-element generator AMEGIC++ [35], an automated implementation [26] of the Catani-Seymour dipole subtraction method [16] and the parton shower model described in [27, 31]. The CTEQ6.6 PDF set [36] is used together with the corresponding parametrisation of the running coupling. All analyses are carried out with the help of Rivet [37].

4.1 Higgs-boson production in gluon fusion

The production of a Higgs boson at the LHC with 7 TeV centre-of-mass energy serves as a first example. This process amplifies some of the effects discussed in Sec. 2.5 because the radiating partons are gluons. There are thus no valence PDF's involved at Born level, which allows to test fixed-order effects and resummation in a relatively clean setting. Results presented in this section do not include non-perturbative or multiple parton scattering effects. A detailed study of the POWHEG algorithm and its associated uncertainties has already been presented in [15]. In the following, the focus will therefore mainly lie on the MC@NLO method, but comparisons with POWHEG will be made at the appropriate junctures.

For an unbiased comparison of the MC@NLO and POWHEG techniques, the events are analysed with a minimal set of cuts. A Higgs-boson mass of $m_h = 120$ GeV is assumed and two τ -leptons with $|\eta| < 3.5$ and $p_\perp > 25$ GeV are required; jets are defined according to the inclusive k_\perp -algorithm [38] with $R = 0.7$ and $p_{\perp, \text{min}} = 20$ GeV. The renormalisation and factorisation scales are set to $\mu_F = \mu_R = m_h$. The effective coupling of the Higgs to gluons, mediated by a top-quark loop, is modeled through an effective Lagrangian [39].

The comparison with fixed-order predictions and predictions from standard parton showers (referred to as LO \otimes PS in the following) presents a first crucial test of the MC@NLO and POWHEG methods. In this context, SHERPA is also used as a framework for NLO fixed-order event generation, enabling a comparison of all approaches with identical input parameters. In order to vary the amount of exponentiated real-emission corrections in MC@NLO, which is governed by Eqs. (2.10)-(2.12) or, more rigorous, Eqs. (3.12)-(3.14), the phase-space restriction described in [40] is employed and the parameter α_{cut} is varied. It has the effect of increasing ($\alpha_{\text{cut}} \rightarrow 1$) or decreasing ($\alpha_{\text{cut}} \rightarrow 0$) the phase space for non-singular contributions in $D^{(A)}$ by setting an upper bound on the virtuality \hat{t} of the splitting parton. The leading logarithm is then of the form $\alpha_s \log^2(\hat{t}/\alpha_{\text{cut}} s)$, with s the centre-of-mass energy of the colliding protons. Hence, for $\alpha_{\text{cut}} \sim 1$ the leading logarithm contains the wrong argument $\alpha_{\text{cut}} s \gg \mu_F^2$, clearly at odds with usual choices of the resummation

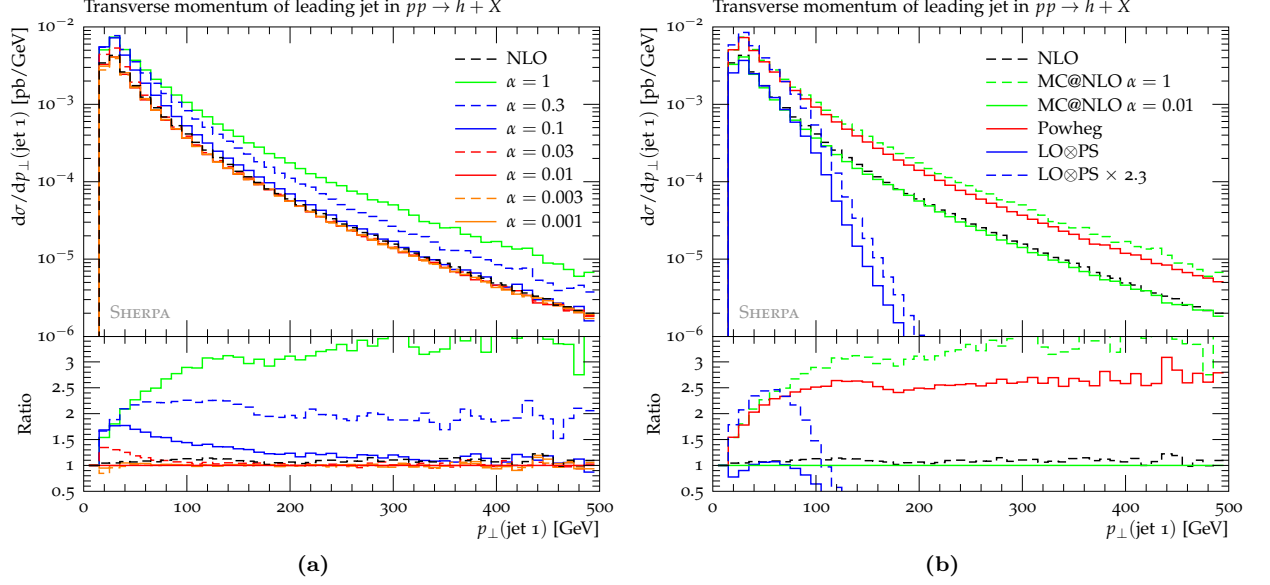


Figure 2: Transverse momentum of the leading jet in inclusive Higgs-boson production ($m_h = 120$ GeV) at $E_{\text{cms}} = 7$ TeV. See Fig. 1 for details.

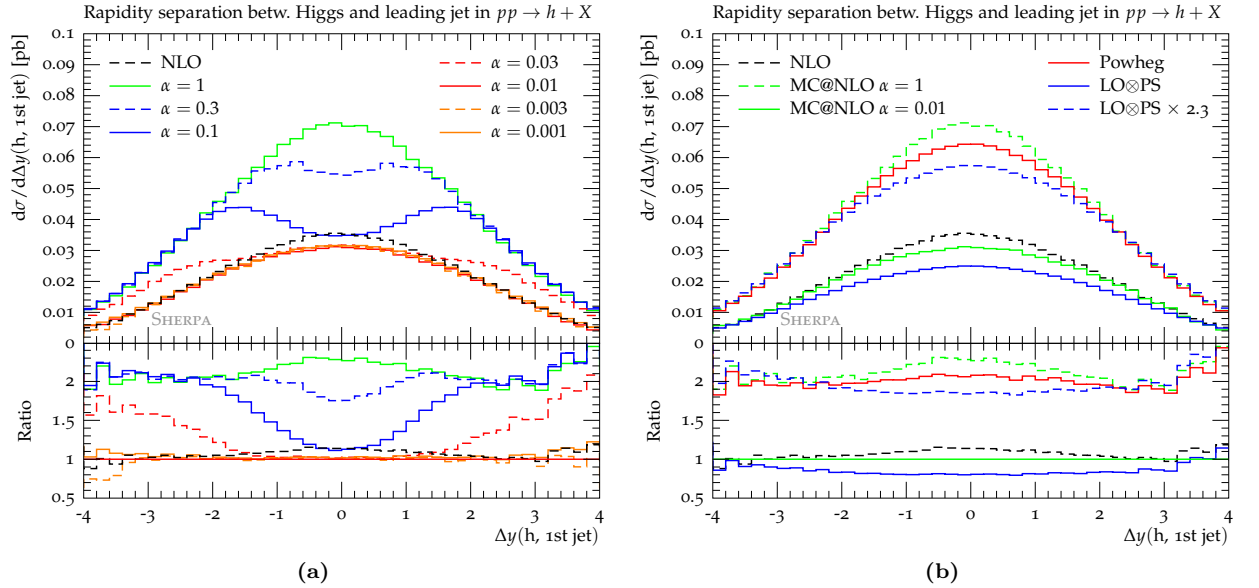


Figure 3: Rapidity separation between Higgs-boson and leading jet in inclusive Higgs-boson production ($m_h = 120$ GeV) at $E_{\text{cms}} = 7$ TeV. See Fig. 1 for details.

scale and in violation of factorisation theorems. Similarly, the original POWHEG method exponentiates radiative corrections throughout the real-emission phase space, corresponding to MC@NLO with $\alpha_{\text{cut}} = 1$. Most of the recent practical implementations of POWHEG choose to suppress non-singular terms with a continuous function which tends to one in the singular limits and approaches zero in those regions of phase space where emissions become hard [7, 15, 19]. However, the volume of phase space where exponentiation is performed is left invariant in this approach, and only the influence of non-logarithmic terms is reduced. The leading logarithm is thus still of the form $\alpha_s \log^2(\hat{t}/s)$. The traditional LO \otimes PS method directly implements the DGLAP resummation and thus uses the factorisation scale μ_F as a phase space constraint, resulting in the correct logarithmic form $\alpha_s \log^2(\hat{t}/\mu_F^2)$.

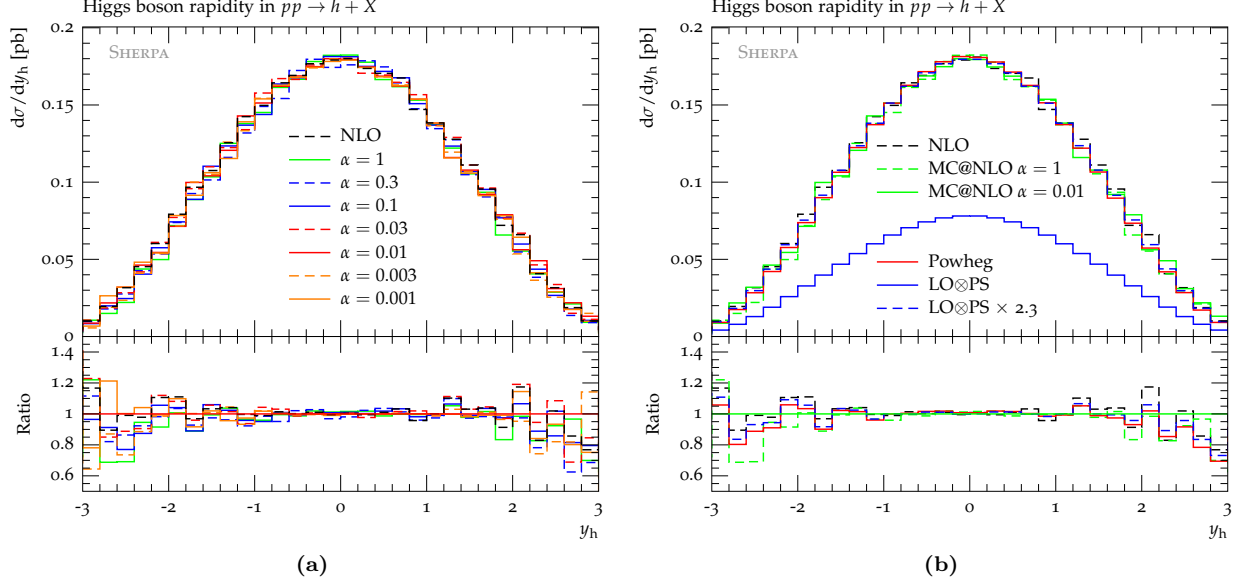


Figure 4: Prediction and uncertainties for the rapidity of the Higgs boson in inclusive Higgs boson production ($m_h = 120$ GeV) at $E_{\text{cms}} = 7$ TeV. See Fig. 1 for details.

The influence of α_{cut} on the MC@NLO predictions and its relation to the POWHEG and LO \otimes PS predictions are investigated for various observables in Figs. 1-4. Taking the $\mathcal{O}(\alpha_s)$ expansion of Eq. (3.13) at face value leads to the expectation that results from MC@NLO (for any α_{cut}) and POWHEG should agree with fixed-order predictions in the limit of hard, well separated partons. In the limit of soft/collinear radiation the common logarithmic structure of the resummation in MC@NLO, POWHEG and LO \otimes PS should lead to identical results in all three approaches.

In practice, the transverse momentum spectrum of the Higgs boson, shown in Fig. 1a, exhibits a large dependence on α_{cut} . This roots in the different composition of the distribution in terms of \mathbb{H} - and \mathbb{S} -events, which is depicted in Figs. 5 and 6. Neglecting subsequent parton shower emissions, \mathbb{H} -events above α_{cut} coincide with those of the NLO calculation, while \mathbb{S} -events resum the leading logarithm of the real emission matrix element and occur with an additional enhancement $\bar{B}^{(A)}/B$. This enhancement, though formally contributing to $\mathcal{O}(\alpha_s^2)$, can be numerically large. Thus, when allowing \mathbb{S} -type events to fill more than the phase space suited for the resummation of the DGLAP logarithms, their emission probability is not only distorted by the exponentiation but also by an artificial K -factor $\bar{B}^{(A)}/B$, as compared to the NLO result. For smaller values of α_{cut} , the argument of the leading logarithm is closer to the one in DGLAP evolution, even though α_{cut} has a functional form which makes a direct comparison difficult. It is thus observed that the MC@NLO distributions come close to the fixed-order result in the hard region, and the method behaves exactly as expected.

Further, excessively small values of α_{cut} lead to spurious results, as the \mathbb{S} -event prefactor $\bar{B}^{(A)}/B$ turns negative. This is exemplified in Fig. 5. Thus, those values of α_{cut} are preferred which ensure that \mathbb{S} -events only fill the phase space suited for resummation and simultaneously avoid $\bar{B}^{(A)}$ turning negative. Defining such an allowed range of α_{cut} introduces an unwanted process dependence into this implementation. Clearly a physically more meaningful definition of phase space constraints will ultimately lead to lifting this uncertainty in the method.

Comparing these results to the predictions of the POWHEG and LO \otimes PS methods, depicted in Fig. 1b, one finds that POWHEG behaves as MC@NLO with $\alpha_{\text{cut}} = 1$, suffering from a too large phase space for exponentiation. On the other hand, the resummation properties of the parton shower are retained. The difference in the actual Sudakov shape can entirely be attributed to the respective size and functional form of the phase-space boundaries. Further, within the region where the standard parton shower is able to fill the phase space (up to $|\hat{t}| = \mu_F^2$), the LO \otimes PS result scaled by a global factor $K = \sigma_{\text{NLO}}/\sigma_{\text{LO}} = 2.3$ is in good agreement with the POWHEG and MC@NLO with $\alpha_{\text{cut}} = 1$ distributions. This is a consequence of the simple form of the virtual corrections resulting in a local K -factor $\bar{B}^{(A)}/B$, that largely coincides with the

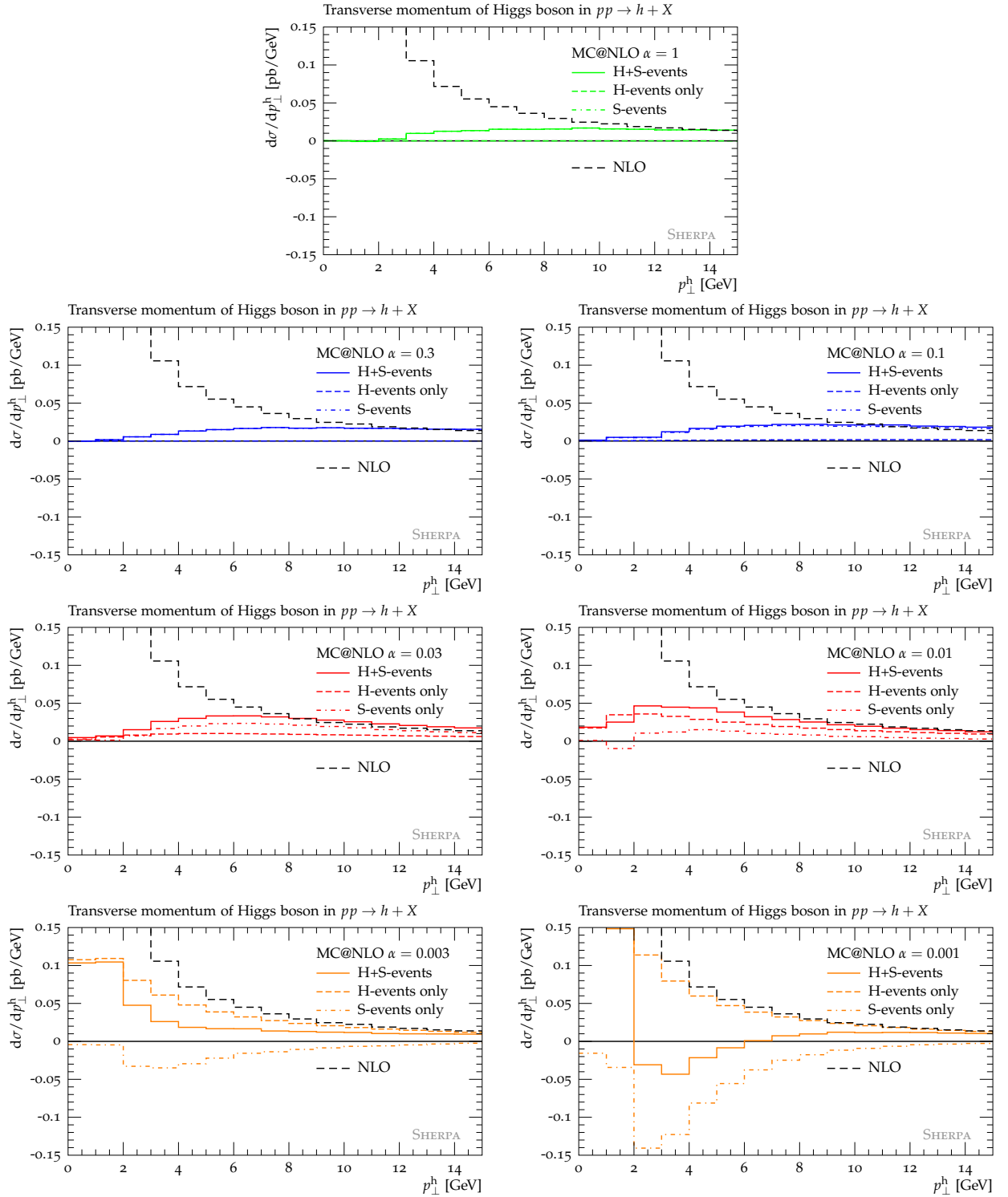


Figure 5: Higgs-boson transverse momentum for small values of p_T^h in inclusive Higgs-boson production ($m_h = 120$ GeV) at $E_{\text{cms}} = 7$ TeV. The contribution of S- and H-events in the MC@NLO method is displayed separately for different values of α_{cut} . For $\alpha_{\text{cut}} = 1$ and $\alpha_{\text{cut}} = 0.3$ the sample consist primarily of S-events with small additions of negatively and positively valued H-events, respectively.

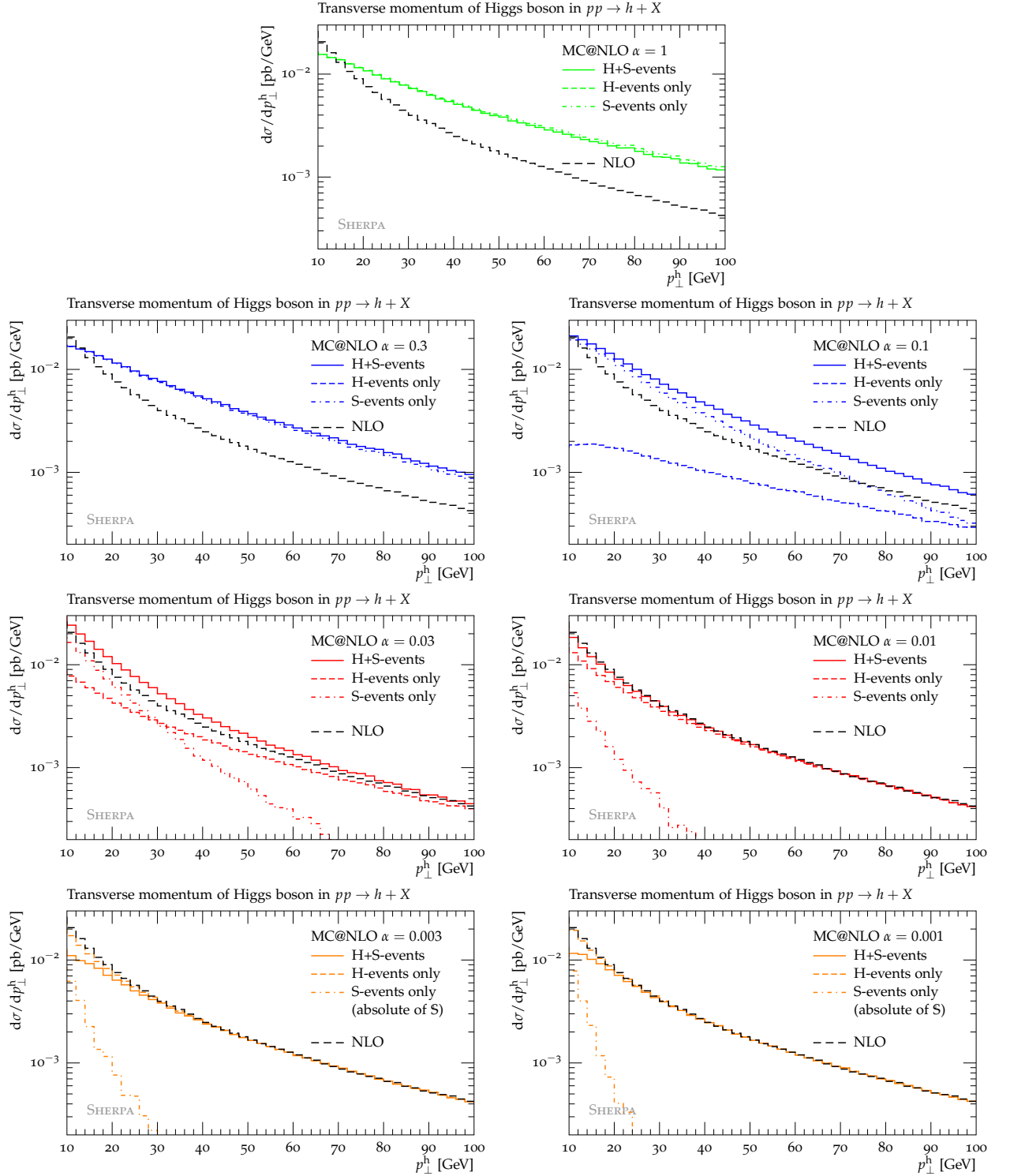


Figure 6: Higgs-boson transverse momentum for large values of p_T^h in inclusive Higgs-boson production ($m_h = 120$ GeV) at $E_{\text{cms}} = 7$ TeV. The contribution of \mathbb{S} - and \mathbb{H} -events in the MC@NLO method is displayed separately for different values of α_{cut} . For $\alpha_{\text{cut}} = 1$ and $\alpha_{\text{cut}} = 0.3$ the sample consist primarily of \mathbb{S} -events with small additions of negatively and positively valued \mathbb{H} -events, respectively.

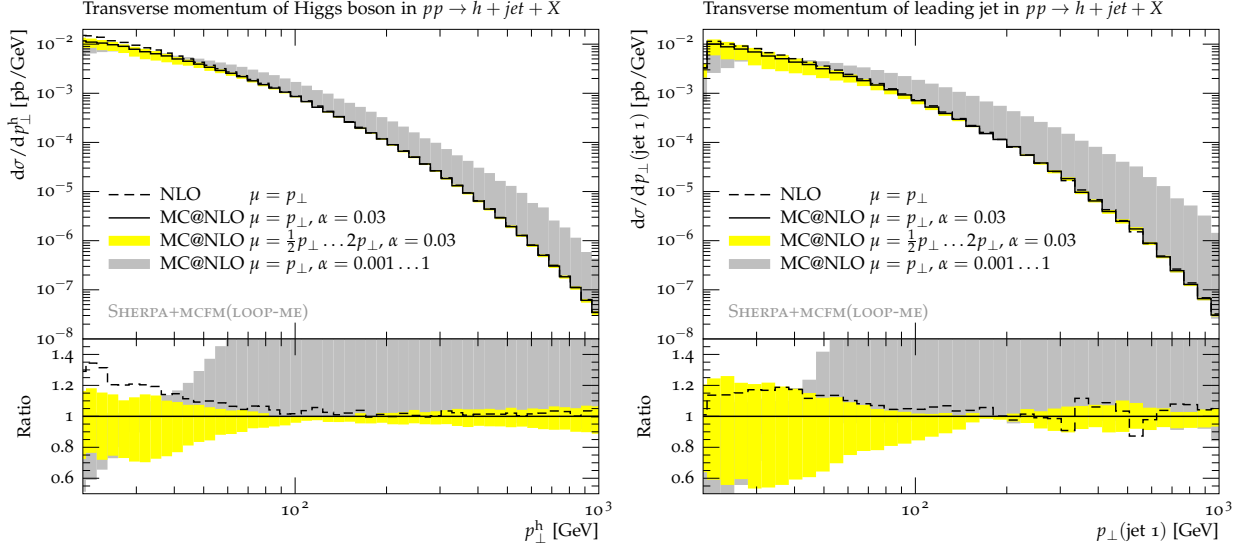


Figure 7: Prediction and uncertainties for the transverse momentum of the Higgs boson (left) and the leading jet (right) in Higgs boson plus jet events ($m_h = 120$ GeV) at $E_{\text{cms}} = 7$ TeV.

global K -factor.

Similar observations are made for the transverse momentum of the hardest jet of Fig 2. Here, the difference in the emission rate for \mathbb{H} - and \mathbb{S} -events, as discussed earlier, is plainly visible. Again, MC@NLO with $\alpha_{\text{cut}} = 0.01$ agrees with the fixed-order NLO prediction for large jet transverse momenta. Also POWHEG and MC@NLO with $\alpha_{\text{cut}} = 1$ give similar results, overestimating the emission rate by more than 250%.

This overestimation also feeds into the rapidity separation between the Higgs boson and the first jet in Fig. 3. The predictions of MC@NLO with $\alpha_{\text{cut}} = 0.01$ and MC@NLO with $\alpha_{\text{cut}} = 1$ differ by a factor of two. The effects of decreasing α_{cut} are examined in Fig. 3a. With decreasing α_{cut} , the rapidity difference distribution develops a pronounced dip, which becomes broader and flattens out until the fixed-order result is approached for $\alpha_{\text{cut}} \approx 0.01$ and stabilises for even smaller α_{cut} . Again, this is explained by the different composition of the samples in terms of \mathbb{H} - and \mathbb{S} -events. Fig. 3b shows comparison with POWHEG and LO \otimes PS. POWHEG predictions agree well with those from MC@NLO with $\alpha_{\text{cut}} = 1$ and from LO \otimes PS with a global K -factor, while MC@NLO with $\alpha_{\text{cut}} = 0.01$ agrees with standard LO \otimes PS.

Fig. 4 shows the rapidity spectrum of the Higgs boson, which can be defined at Born level and is thus described at NLO accuracy. No significant variation is observed in this spectrum when the parameter α_{cut} is varied, as expected. One can thus conclude that both the MC@NLO and POWHEG techniques are consistently implemented in the event generator SHERPA. However, the associated perturbative uncertainties are large.

4.2 Higgs-boson production in association with a jet

This section presents predictions for the production of a Higgs boson in association with at least one jet. This process has not yet been investigated using either the MC@NLO or the POWHEG approach. The Higgs mass is set to $m_h = 120$ GeV. Jets at parton-level (i.e. before parton shower emissions take place) are defined using the inclusive k_\perp algorithm [38] with $R = 0.5$ and $p_{\perp, \text{min}} = 10$ GeV. Again, the effective coupling of the Higgs to gluons, mediated by a top-quark loop, is modeled through an effective Lagrangian [39], and the virtual matrix elements here are computed by MCFM [41].

Both the renormalisation and factorisation scales are set to the transverse momentum of the hardest parton-level jet in the event. For the central prediction $\alpha_{\text{cut}} = 0.03$ is chosen to minimise the uncontrolled exponentiation of non-logarithmic terms and distortions of the Sudakov shape of the Higgs boson's transverse momentum spectrum. The predictions presented here include simulation of hadronisation [42] and multiple parton interactions (MPI) [43] as well as hadron decays [44] and higher-order QED corrections to the $h \rightarrow \tau\tau$ decay [45].

Uncertainty bands correspond to the variation of the renormalisation and factorisation scales in the range

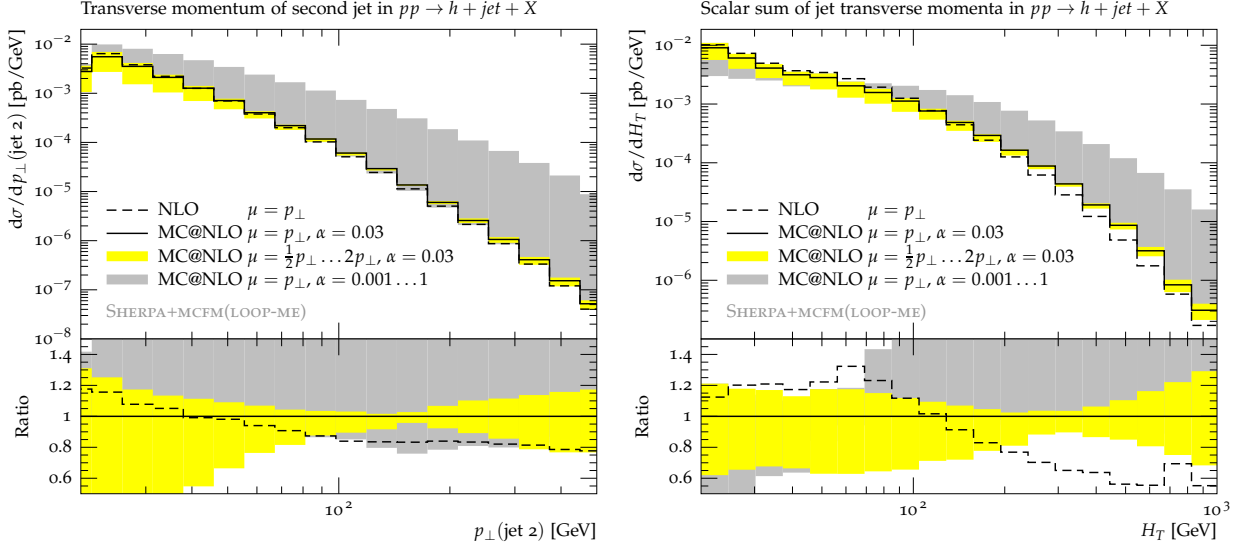


Figure 8: Predictions and uncertainties for transverse momentum of the second hardest jet (left) and the scalar sum of all jet transverse momenta (right) in Higgs boson plus jet events ($m_h = 120$ GeV) at $E_{\text{cms}} = 7$ TeV.

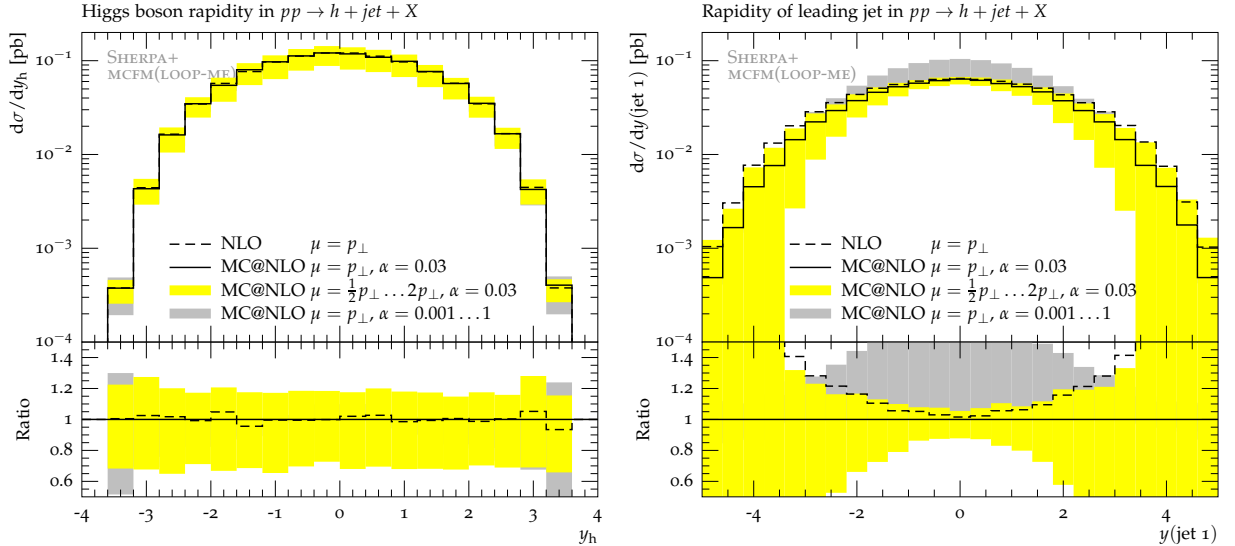


Figure 9: Prediction and uncertainties for the rapidity of the Higgs boson (left) and the leading jet (right) in Higgs boson plus jet events ($m_h = 120$ GeV) at $E_{\text{cms}} = 7$ TeV.

$1/2\mu \dots 2\mu$ as well as to the variation of α_{cut} in a range from 1 to 0.001. As before, only minimal cuts are applied in the analysis: two τ -leptons with $|\eta| < 3.5$ and $p_{\perp} > 25$ GeV are required. Jets are defined using the inclusive k_{\perp} -algorithm with $R = 0.7$ and $p_{\perp, \text{min}} = 20$ GeV. Their minimum transverse momentum requested in the analysis ensures that the parton-level event selection is inclusive enough to guarantee coverage of the full phase space.

Figure 7 shows the transverse momentum spectra of the Higgs boson and the leading jet. Grey bands indicate the uncertainty due to the choice of α_{cut} , which will be referred to as exponentiation uncertainty in the following. Yellow bands show the scale uncertainty. It is manifest, that the exponentiation uncertainty is largest in the region of large transverse momenta, a fact that seems counter-intuitive at first. Despite the transverse momentum distributions being described at NLO, they can apparently be altered significantly by additional emissions in the parton shower. Taking a closer look at Eqs. (2.10)-(2.12), this fact becomes clear:

- The proof of next-to-leading order accuracy of both the POWHEG and the MC@NLO formulae is based

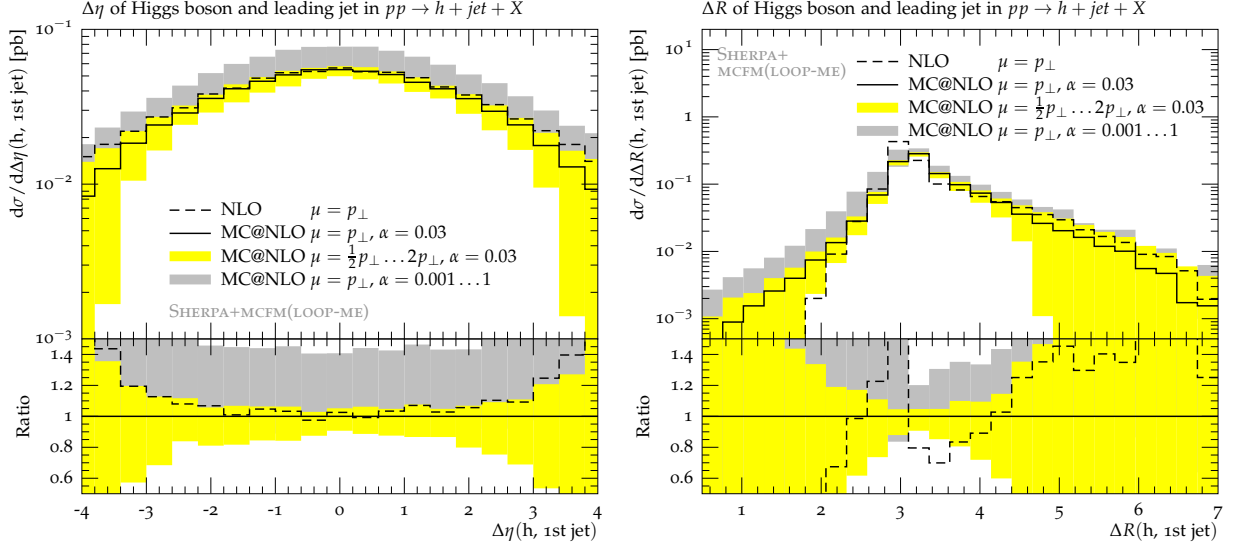


Figure 10: Predictions and uncertainties for the pseudorapidity (left) and angular (right) separation of the Higgs boson and the leading jet in Higgs boson plus jet events ($m_h = 120$ GeV) at $E_{\text{cms}} = 7$ TeV.

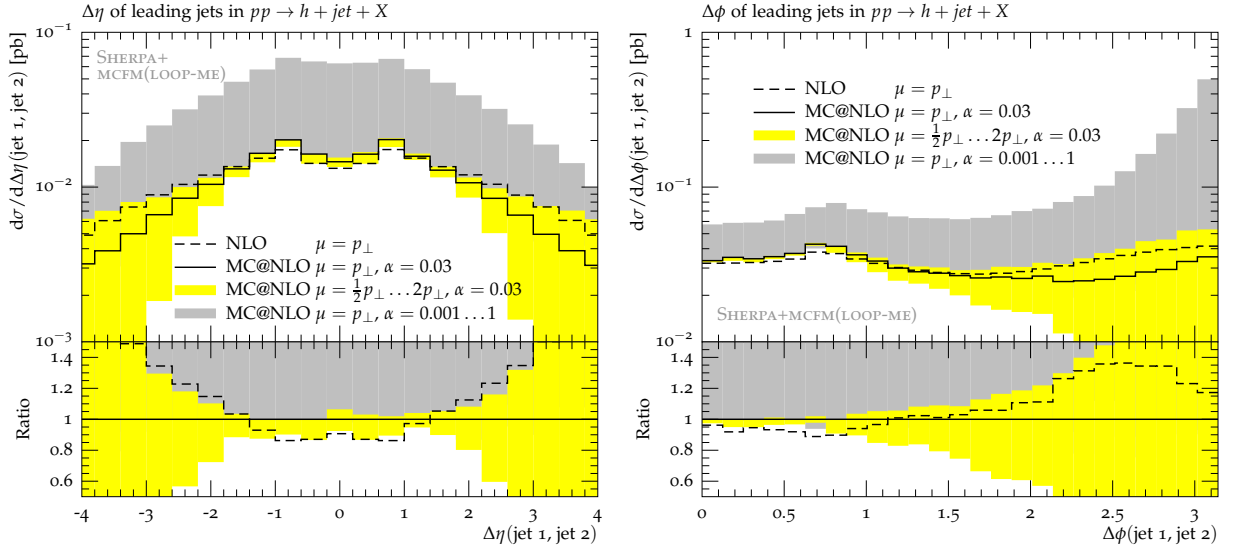


Figure 11: Predictions and uncertainties for the pseudorapidity (left) and azimuthal (right) separation of the two hardest jets in Higgs boson plus jet events ($m_h = 120$ GeV) at $E_{\text{cms}} = 7$ TeV.

on an expansion of the Sudakov form factors to first order. Higher-order corrections do play an important role, however, especially in regions of the phase space where parton emission is logarithmically enhanced. This region is drastically enlarged if the upper integration limit of the exponentiated real emission is shifted from μ_F to $s = E_{\text{CMS}}^2$, as is the case in POWHEG and MC@NLO with $\alpha_{\text{cut}} = 1$ (cf. Sec. 4.1). This change alters the shape of the emission term in Eq. (2.10) compared to the emission term in Eq. (2.9). This finding is reinforced by the fact that in all distributions investigated, the predictions for $\alpha_{\text{cut}} = 0.03$ coincide with those for $\alpha_{\text{cut}} = 0.001$.

- The strong coupling is evaluated at a scale of the order of the relative transverse momentum between two partons in the emission term in Eq. (2.9), while it is evaluated at a different scale (here the transverse momentum with respect to the beam) in Eq. (2.11). This leads to an additional distortion of the spectrum of the real-emission term, which is formally a sub-leading effect, but which becomes important in the enlarged logarithmically enhanced regions of the emission phase space.

The above effects are amplified in Fig. 8, as the observables there, the transverse momentum of the second

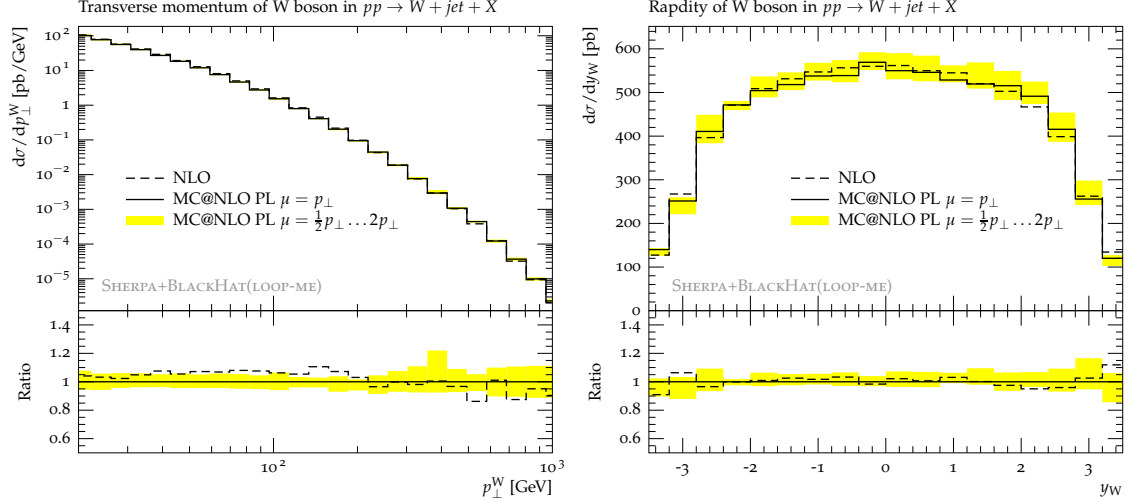


Figure 12: Transverse momentum and rapidity of the W -boson in $W[\rightarrow e\nu] + j$ production at the LHC.

jet and the scalar sum of all jets in the event, are described at leading-order accuracy only.

In contrast, Figs. 9 and 10 show a rather mild dependence on α_{cut} in the shape of the distributions. Nonetheless, a change in the normalisation can be observed, which is explained by the fact that due to larger emission rates with increasing α_{cut} , the amount of radiative events is increased. Their kinematic distribution, however, does not seem to differ significantly. In fact, the large scale dependence observed in Figs. 7 and 8 is amplified here, especially for observables related to the hardest jet, indicating that, although $\mu = p_{\perp}$ is an appropriate scale choice for this process, the canonical variation to $\mu = \frac{1}{2}p_{\perp}$ leads to unphysical behaviour for jet rapidities beyond $|\eta| \approx 3.4$.

As a consequence of the strongly varying jet rates with varying α_{cut} , the pseudorapidity separation between first and second hardest jet suffers from large uncertainties. It is displayed in Fig. 11. While the shape of the distribution is mostly unaffected, the normalisation varies strongly. The azimuthal separation between the two leading jets indicates how the exponentiation uncertainty affects the relative position of both jets in phase space. Compared to the pure next-to-leading order result, the back-to-back situation is amplified by a factor ~ 10 in the MC@NLO prediction. In such events, the Higgs-boson is likely to have been produced at $p_{\perp} \rightarrow 0$, consistent with the observation of a depletion of events in the first bins of the Higgs transverse momentum spectrum for $\alpha_{\text{cut}} = 1$, cf. Fig. 7.

4.3 W -boson production in association with a jet

In the following, $W[\rightarrow e\nu] + \text{jet}$ production in pp collisions at 7 TeV is studied. As for the case of Higgs-boson production, the MC@NLO implementation is validated against a fixed-order calculation. In addition the scale uncertainties are assessed by varying factorisation and renormalisation scales in MC@NLO by a factor of two in both directions.

To make the validation as meaningful as possible effects from parton showering beyond the first emission in S -events, hadronisation and multiple parton scattering are not included in these parton level (PL) studies. Events are generated requiring at least one jet with $p_{\perp, \text{min}} = 10$ GeV, defined according to the inclusive k_{\perp} -algorithm [38] with $R = 0.5$. The transverse momentum of that hardest jet also sets the central value of factorisation and renormalisation scales. The level of exponentiation is fixed by $\alpha_{\text{cut}} = 0.03$.

The total generated cross sections of the NLO calculation, $\sigma_{\text{NLO}} = (4695 \pm 12)$ pb, and MC@NLO, $\sigma_{\text{MC@NLO}} = (4680 \pm 30)$ pb, agree within statistical uncertainties. The total generated cross section in MC@NLO varies between $\sigma(\mu/2) = (4950 \pm 40)$ pb and $\sigma(\mu \cdot 2) = (4510 \pm 23)$ pb, i.e. up to 5.8% around the central value.

Properties of the W -boson, which is reconstructed from the truth neutrino and the lepton, are displayed in Fig. 12. Agreement between fixed-order and MC@NLO results in both the rapidity and transverse momentum spectra is found. Agreement is also found for the transverse momentum and pseudorapidity distributions of the electron, which are shown in Fig. 13.

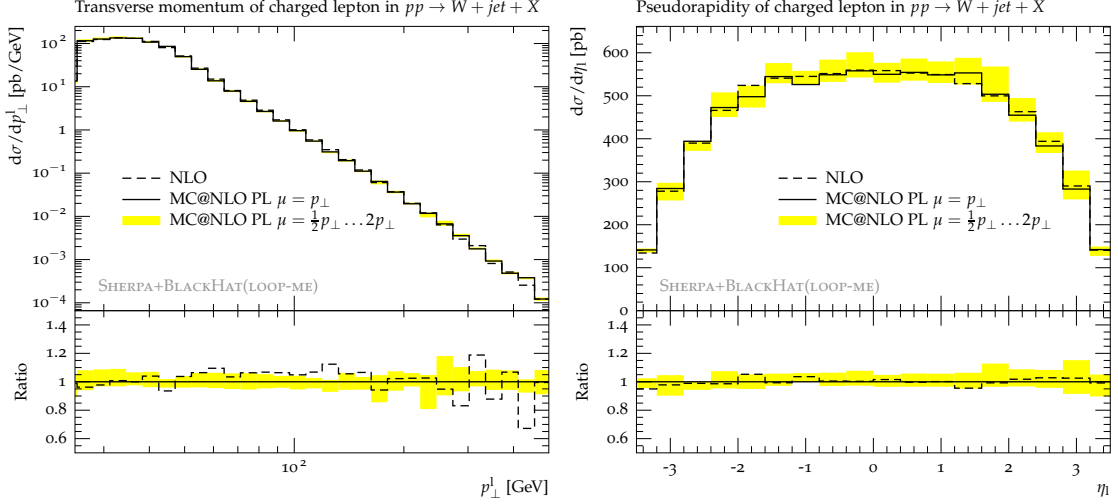


Figure 13: Transverse momentum and pseudorapidity of the electron in $W[\rightarrow e\nu] + j$ production at the LHC.

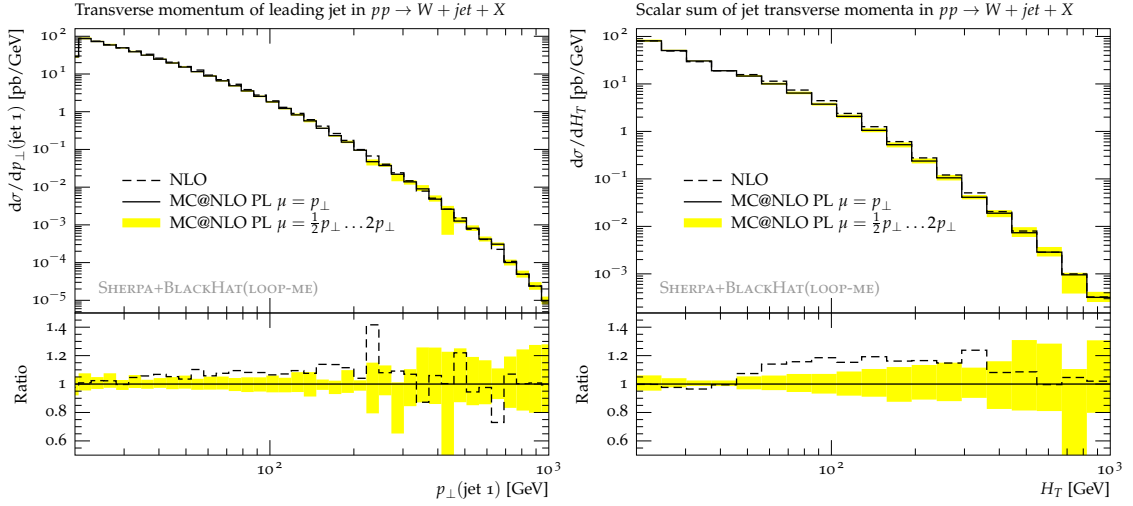


Figure 14: Transverse momentum of the leading jet and scalar sum of all jet transverse momenta in $W[\rightarrow e\nu] + j$ production at the LHC.

In the event analysis jets are defined according to the inclusive k_\perp algorithm [38] with $R = 0.7$ and requiring $p_\perp > 20$ GeV. Properties of these jets are displayed in Fig. 14. The transverse momentum of the leading jet, an observable described at next-to-leading order accuracy, shows good agreement between both approaches. The scalar sum of jet transverse momenta (H_T) is only described at leading-order accuracy and thus suffers from larger exponentiation uncertainties. This leads to a disagreement between the fixed-order result and MC@NLO, up to the level of 20%.

No distribution is affected significantly by scale variations beyond the change in total rate. This indicates that the functional form of the scale choice described at the beginning of this section works well for this process.

5 Non-perturbative uncertainties and comparison to data

In this section the MC@NLO method is further studied using W +jet and Z +jet production as a testing ground. Emphasis is now placed on the investigation of non-perturbative effects and associated systematic variations.

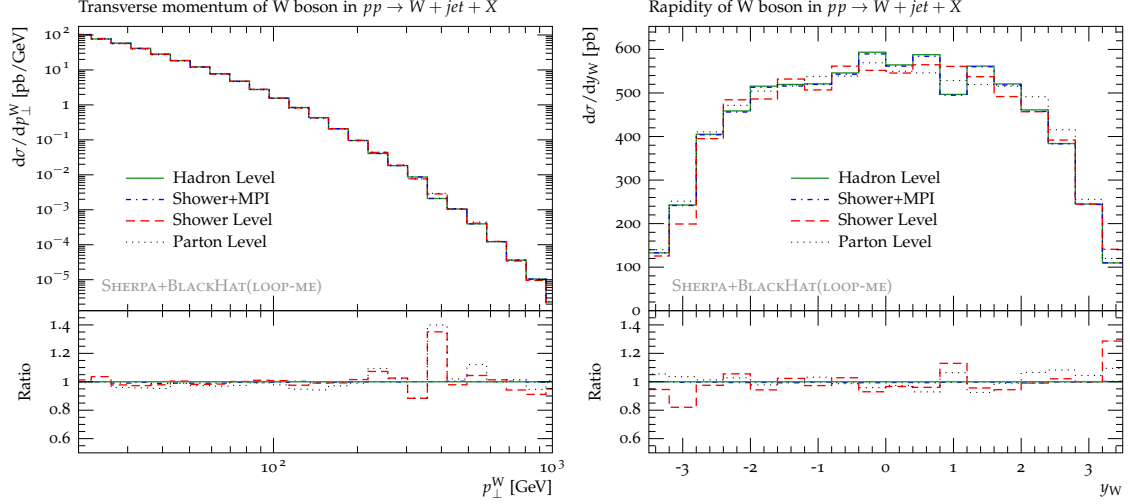


Figure 15: Transverse momentum and rapidity spectrum of the W -boson in $W[\rightarrow e\nu] + j$ production at the LHC.

5.1 Analysis of non-perturbative effects

The MC@NLO method allows to generate fully hadronised events as an input for detector simulation or for direct comparison to measurements at the particle level. A question that naturally arises is, whether the theoretical uncertainties of the full MC@NLO simulation are then dominated by the perturbative or non-perturbative effects. We do not attempt to judge on this question here as it is not obvious on which grounds they can be compared at all, but rather point out that both non-perturbative corrections and non-perturbative uncertainties are modest compared to the intrinsic uncertainties of the parton-level result, which were investigated in the previous section.

To this end, MC@NLO simulations for W +jet production are compared with a varying level of non-perturbative effects included:

“Parton Level”

Only the first emission off S -events in MC@NLO is generated in addition to the seed event. This is the same method that was used in the comparison to fixed-order results in Sec. 4.3.

“Shower Level”

All QCD emissions in the parton shower and QED emissions in the YFS approach are taken into account.

“Shower+MPI”

Multiple parton interactions and intrinsic transverse momentum of the beam hadron are additionally allowed for.

“Hadron Level”

Hadronisation and hadron decays are included to generate events at the particle level.

All other event generation parameters have been chosen identical to Sec. 4.3.

Non-jet observables, like the rapidity and transverse momentum of the W -boson and the rapidity and transverse momentum of the charged lepton are virtually unaffected by non-perturbative effects, as expected. This is shown in Figs. 15 and 16.

Jet observables are far more sensitive, as is exemplified by the transverse momentum and rapidity spectra of the leading and next-to-leading jet in Fig. 17. They show effects of “out-of-cone” radiation at shower level, which are partially compensated by the simulation of multiple scattering effects. Hadronisation again leads to softer jet spectra, such that the various effects can compensate each other. Although the tendency of the corrections stays the same, their precise magnitude depends on the jet algorithm and its parameters and will have to be investigated separately for each analysis. Figure 18 exemplifies how non-perturbative effects can distort correlations between the two hardest jets.

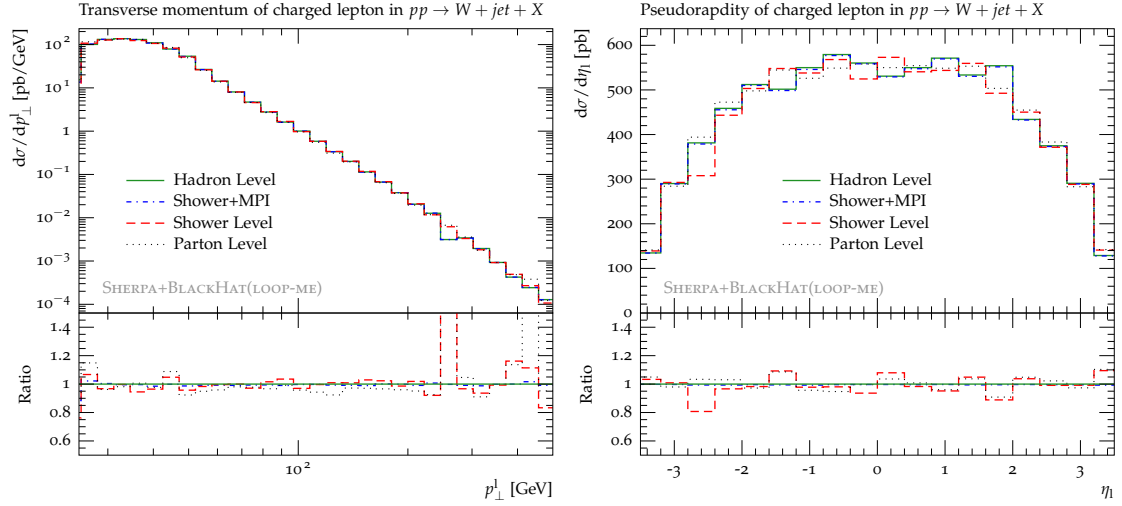


Figure 16: Transverse momentum and pseudorapidity spectrum of the electron in $W[\rightarrow e\nu] + j$ production at the LHC.

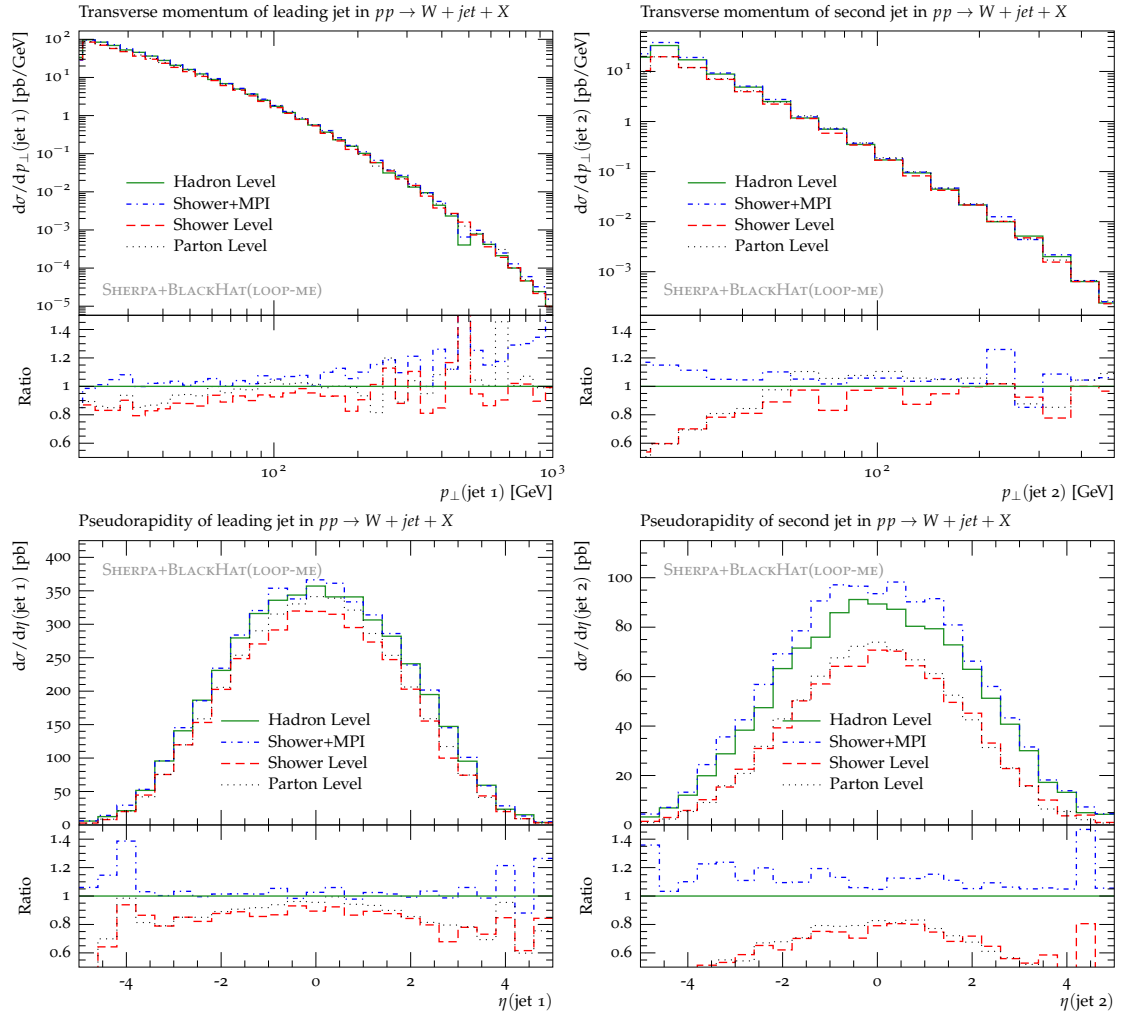


Figure 17: Transverse momenta and pseudorapidities of the two leading jets in $W[\rightarrow e\nu] + j$ production at the LHC.

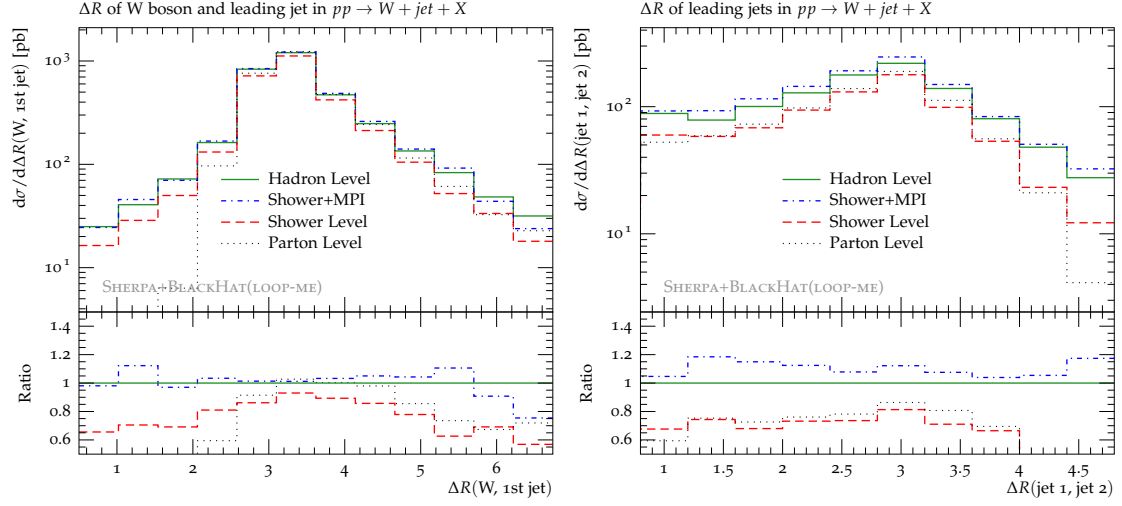


Figure 18: Correlations between W -boson and leading jets in $W[\rightarrow e\nu] + j$ production at the LHC.

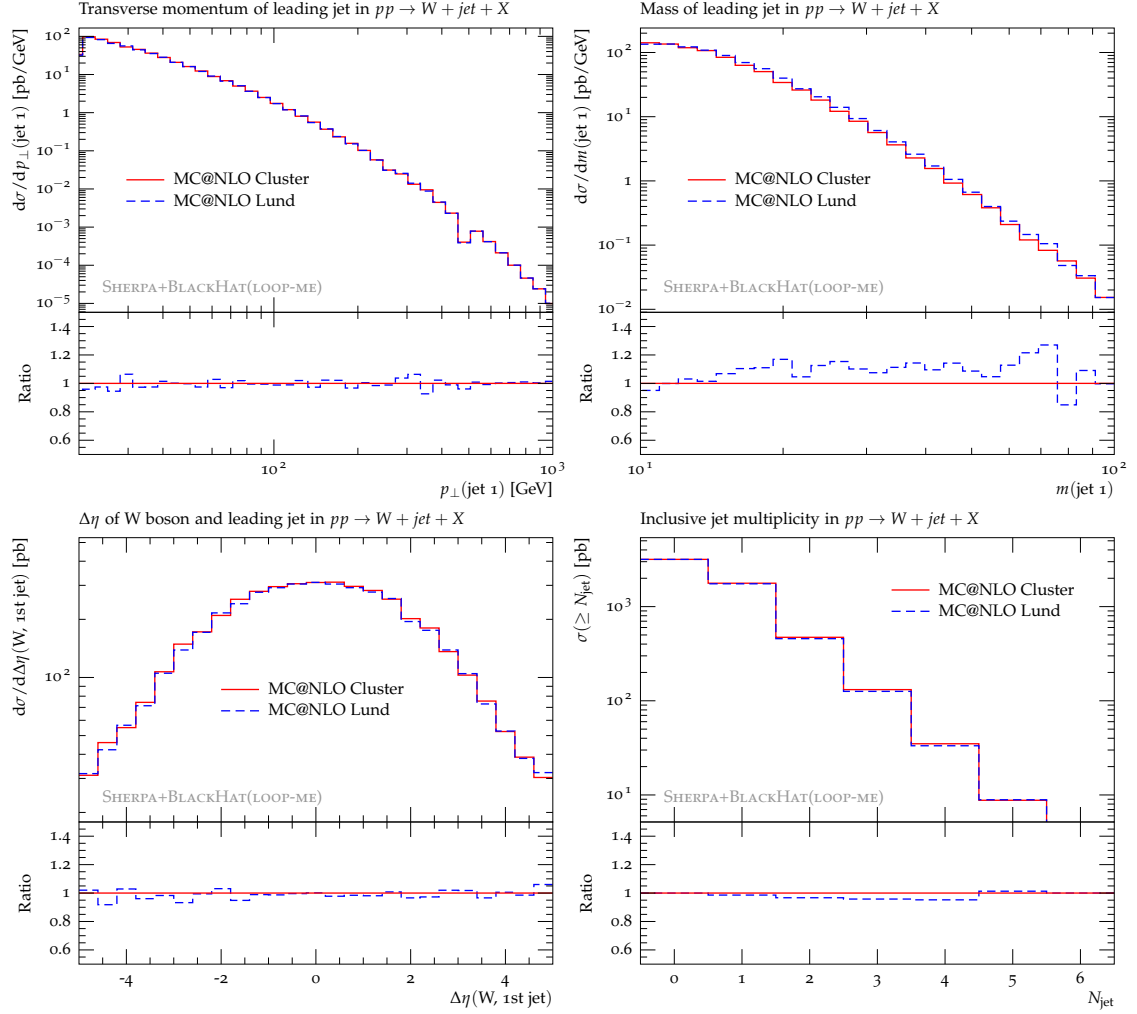


Figure 19: Hadronisation uncertainties for different observables studied in $W[\rightarrow e\nu] + j$ production at the LHC.

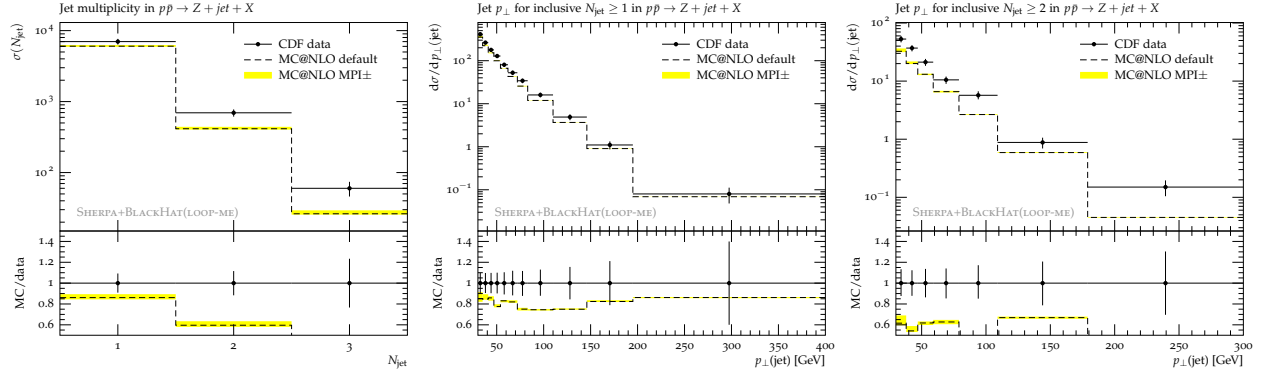


Figure 20: Inclusive jet cross sections and inclusive transverse momentum distributions of all and all-but-the-hardest jets compared to CDF data [47].

The uncertainties inherent in the hadronisation model were probed by switching from the SHERPA default cluster fragmentation model [42] to the Lund string model [46] in the implementation of PYTHIA [33]. Both models have been tuned to data from LEP and excellent agreement has been achieved. For this comparison to be meaningful the same perturbative events (i.e. identical random seeds) were subjected to the two hadronisation models. Effects from statistical fluctuations are thus cancelled.

The differences were found to be negligible for the observables studied here, as displayed in Fig. 19, except for the specifically hadronisation-sensitive jet mass, where variations up to 20% occur.

5.2 Z +jet production compared to Tevatron data

Let us now turn to the comparison of MC@NLO predictions to data and a simple assessment of the systematic uncertainties associated with a significant part of the non-perturbative effects. Central predictions are made at the hadron level with SHERPA’s default tune. An uncertainty band is generated by allowing for a variation of the MPI parameters within boundaries given by existing measurements of the underlying event. All event generation parameters have been chosen analogous to the W +jet case above.

Figure 20 compares Z +jet production in the electron channel to a measurement from the CDF collaboration [47]. The reconstructed electrons are required to have transverse momenta $p_\perp > 25$ GeV and an invariant mass of $66 < m_{ee} < 116$ GeV. Jets are defined using the midpoint cone algorithm [48] with $R = 0.7$ and a split/merge fraction of 0.75. At least one jet with $p_\perp > 30$ GeV and $|y| < 2.1$ needs to be present and separated from both electrons by $\Delta R_{ej} > 0.7$. The cross section in the one-jet bin is predicted slightly too low. The cross section of the two-jet bin is significantly underestimated, as it is determined to leading order accuracy and subject to large uncertainties from the NLO+PS matching procedure as discussed in Sec. 4. The shape of the transverse momentum distributions agrees well with data.

More characteristics of Z -boson plus jet production were investigated in a recent $D\bar{O}$ analysis [49]. Events with two muons of invariant mass $65 < m_{\mu\mu} < 115$ GeV and with at least one jet of $p_\perp > 20$ GeV and $|y| < 2.8$ were collected at a center-of-mass energy of 1.96 TeV. Jets were defined using the $D\bar{O}$ midpoint cone algorithm [50] with $R = 0.5$ and a split/merge fraction of 0.5. Each jet had to be separated from both leptons by $\Delta R_{\mu j} > 0.5$. A comparison of Monte-Carlo predictions with this measurement is shown in Fig. 21. The agreement is fair, except for the p_\perp -spectrum of the first jet, where a deficiency of the Monte-Carlo result at intermediate and high p_\perp is observed.

A further measurement of Z +jet production in the electron channel was presented by the $D\bar{O}$ collaboration in [51]. Each electron is required to have $p_\perp > 25$ GeV and the mass window $65 < m_{ee} < 115$ GeV is enforced. Jets are defined using the midpoint cone algorithm [50] with $R = 0.5$ and a split/merge fraction of 0.5. At least one jet with $p_\perp > 20$ GeV and $|\eta| < 2.5$ must be present in the event. Experimental data were normalised to the inclusive Drell-Yan cross section. This quantity is not predicted by the MC@NLO simulation of Z +jet, and therefore the MC@NLO results are scaled by a global factor of 0.35 such that the normalisation of the one-jet-rate agrees with data. Figure 22 displays the comparison of these scaled MC@NLO predictions with the results from $D\bar{O}$. The transverse momentum shape of the leading jet is well described by the simulation. The two-jet rate, described here at leading-order accuracy, seems to be

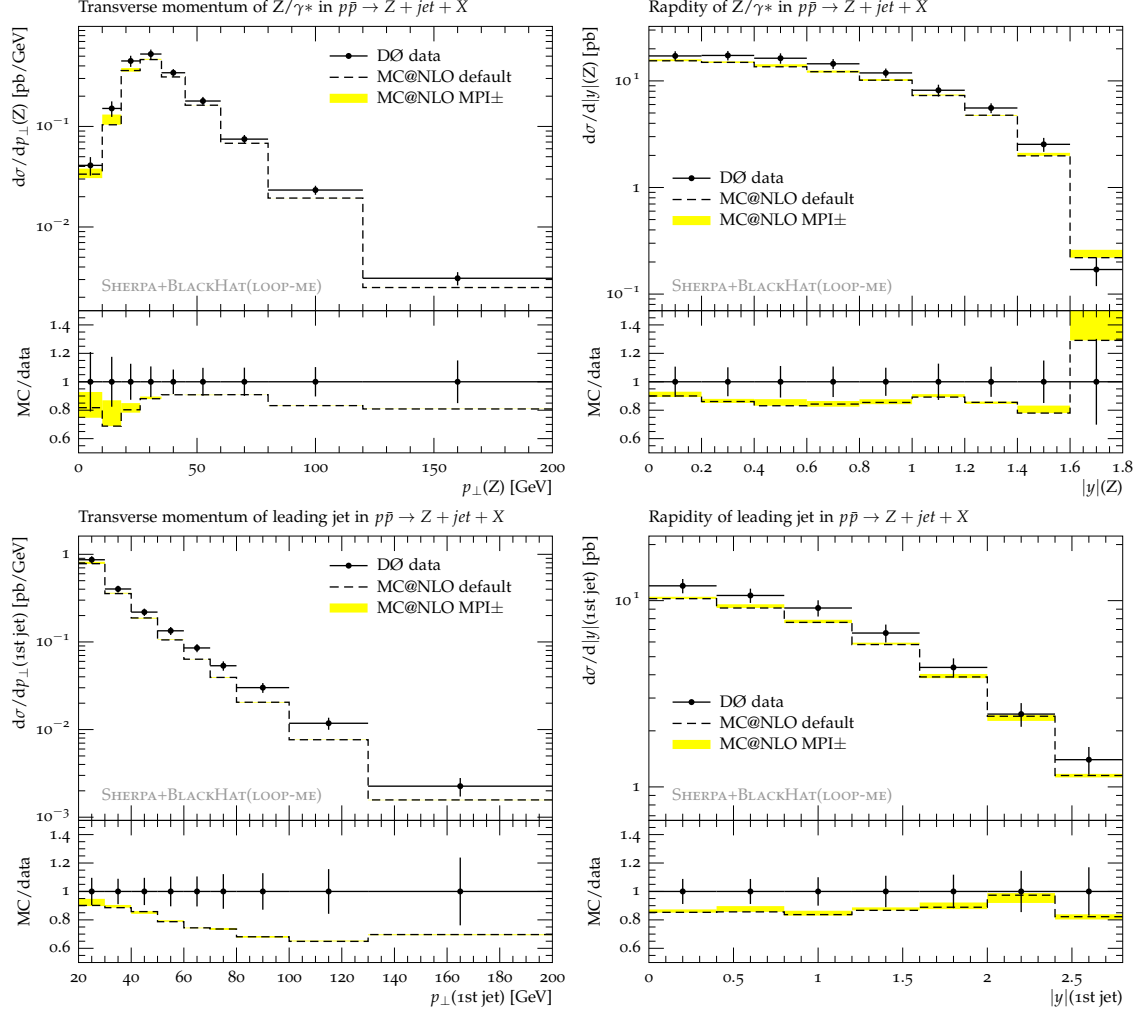


Figure 21: Transverse momentum and rapidity distributions of the reconstructed Z boson (top row), and the total cross section, the transverse momentum and rapidity distributions of the hardest jet (bottom row) in Drell-Yan production in association with at least one jet compared to DØ data [49].

underestimated compared to data, but the shape of the sub-leading jet's p_\perp spectrum is relatively flat. For the third jet, which is generated in the parton-shower approximation, both the rate and the shape of the spectrum are not simulated correctly.

To quantify the success of the next-to-leading order calculation it is important not only to investigate single-particle spectra, but also correlations between the Z -boson and the hardest jet. They might give some insight into the genuine one-loop effects in Z +jet production. Therefore, the analysis strategy of a measurement presented by the DØ collaboration in [52] is pursued. Opposite-sign muons with $p_\perp > 15$ GeV and an invariant mass of $65 < m_{\mu\mu} < 115$ GeV are required in association with at least one jet of $p_\perp > 20$ GeV and $|y| < 2.8$. Jets are defined using the midpoint cone algorithm [50] with $R = 0.5$ and a split/merge fraction of 0.5. Two event samples are defined, one requiring the transverse momentum of the reconstructed Z boson to be above 25 GeV, the other requiring it to be above 45 GeV. Figure 23 compares MC@NLO predictions to the measurement. The shape of the rapidity distributions is matched fairly well, again with the total rate prediction at the lower end of the uncertainty band. For the azimuthal correlation distribution the shape shows significant deviations from data: Only the back-to-back configuration is described well, but for $\Delta\phi < \pi$ the MC@NLO prediction underestimates the data. This signals the uncertainty related to emissions beyond the hardest one, which are only generated at leading-order or parton-shower accuracy and which are also subject to large NLO+PS matching systematics as discussed in Sec. 4.

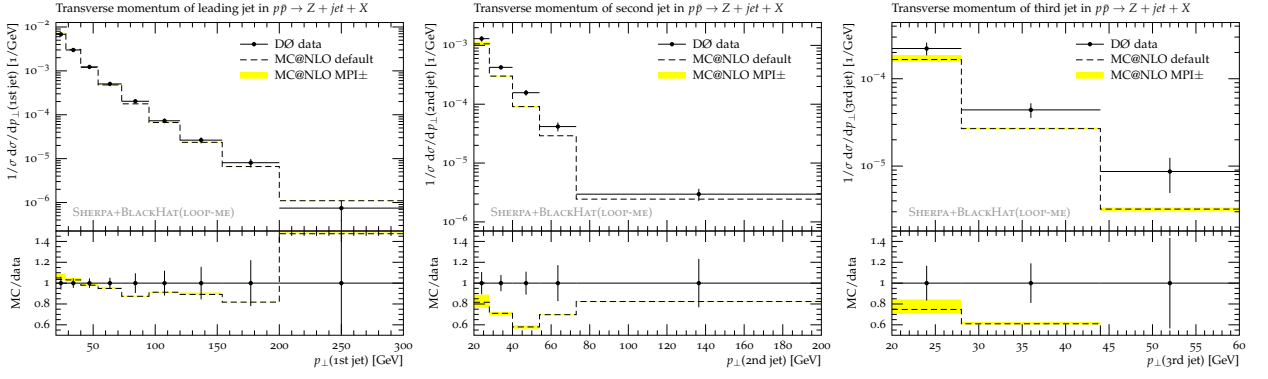


Figure 22: Transverse momentum distributions of the three hardest jets in Drell-Yan production in association with at least one jet compared to DØ data [51]. All SHERPA predictions are scaled by a common factor to account for the unknown normalisation to the inclusive process.

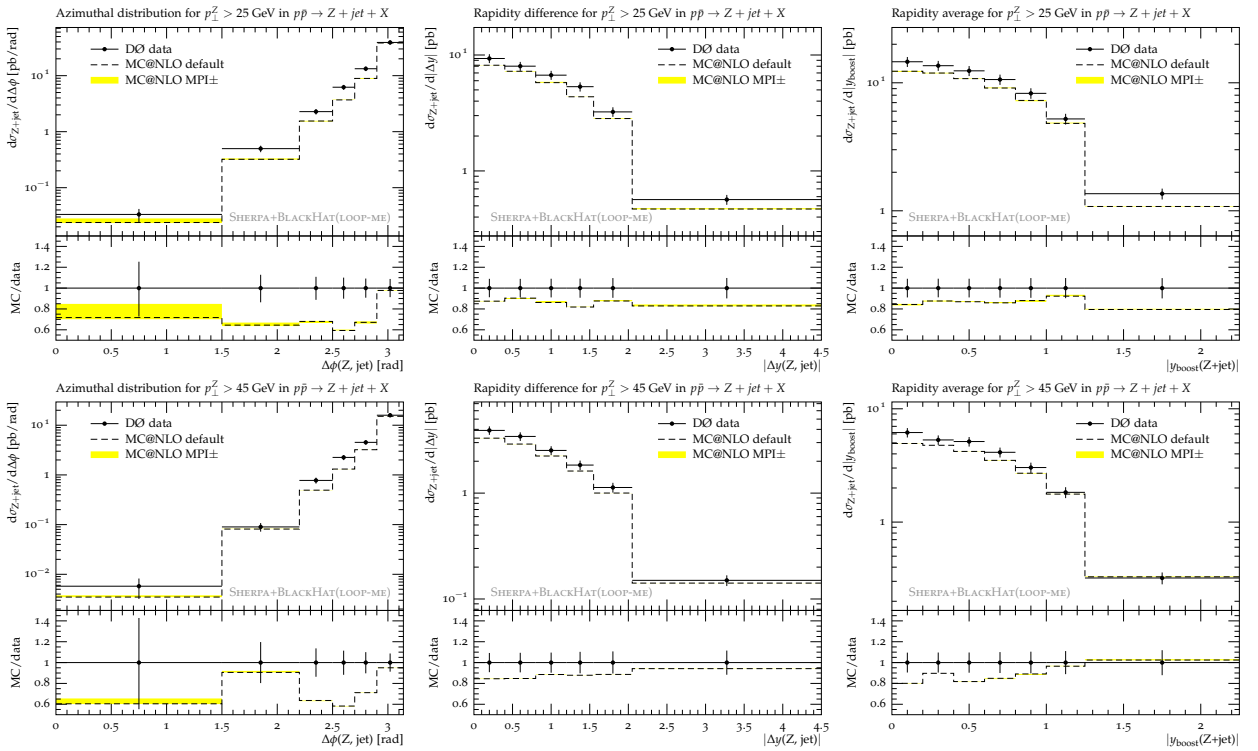


Figure 23: Azimuthal and rapidity difference distributions of the reconstructed Z boson and the hardest jet and their rapidity average in Drell-Yan production in association with at least one jet compared to DØ data [52].

5.3 W +jet production compared to LHC data

The production of a W boson in association with at least one hard jet in proton-proton collisions at $\sqrt{s} = 7$ TeV has been studied by the ATLAS collaboration at the CERN LHC [11].

In the electron channel events are selected by requiring an electron with $p_{\perp} > 20$ GeV defined at the particle level to include all photon radiation within a $\Delta R = 0.1$ cone. Only electrons in the fiducial volume $|\eta| < 1.37$ or $1.52 < |\eta| < 2.47$ are taken into account. E_{\perp}^{miss} at the particle level has been defined through the leading neutrino in the event which is required to have $p_{\perp, \nu} > 25$ GeV. The transverse mass cut is placed at $m_T = \sqrt{2p_{\perp}^{\ell} p_{\perp}^{\nu} (1 - \cos(\phi_{\ell} - \phi_{\nu}))} > 40$ GeV.

Jets are reconstructed using the anti- k_t algorithm with $R = 0.4$ and have been taken into account if $p_{\perp}^{\text{jet}} >$

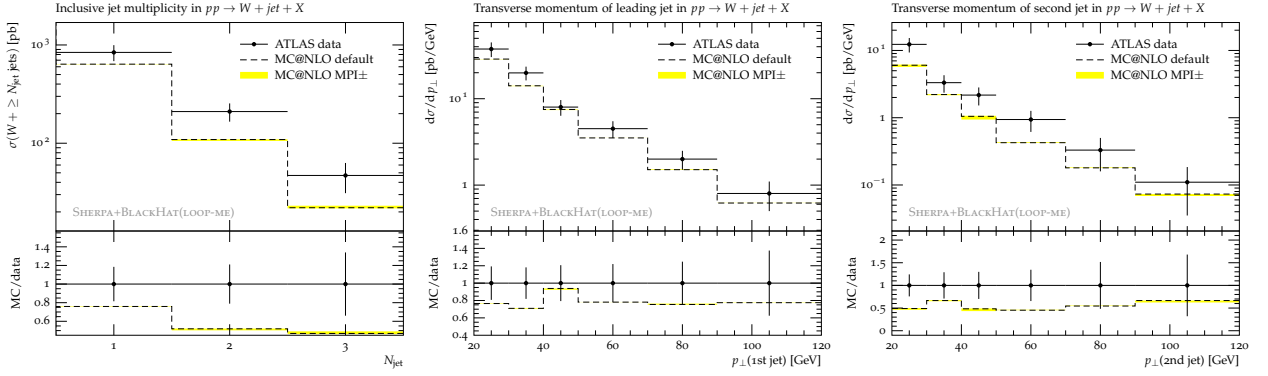


Figure 24: Inclusive jet cross sections and transverse momentum spectra of the hardest and second hardest jet in $W[\rightarrow e\nu] + j$ production at the LHC compared to ATLAS data [11].

20 GeV, $|\eta_{\text{jet}}| < 2.8$ and $\Delta R(\ell, \text{jet}) > 0.5$. Muons, neutrinos and the leading electron were excluded from the input of jet reconstruction.

The comparison in Figure 24 shows good agreement of the SHERPA hadron level prediction with ATLAS data in the shapes of differential distributions on the one hand, and discrepancies in the prediction of the total rate on the other hand. While the one-jet rate is still predicted fairly well, the two and three-jet rates are significantly too low. The latter are only predicted at leading-order and parton-shower accuracy and also subject to the inherent uncertainties from NLO+PS matching.

6 Conclusions

In this publication, the MC@NLO and POWHEG methods to match NLO QCD matrix elements with parton showers have been compared, with a special emphasis on some issues left open in the literature. In particular, these issues are related to

- linking R and B in POWHEG
- the treatment of sub-leading colour configurations in MC@NLO
- the choice of scales in POWHEG and MC@NLO
- the exponentiation of non-leading terms in POWHEG and
- the restriction of the radiative phase space in MC@NLO.

Before discussing the findings related to these issues, it is worth summarising some other results presented in this publication. They refer to the impact of scale variations at the parton-level of the processes studied here, and to the effect of hadronisation and the underlying event on a number of observables:

- **Scale uncertainties**
In $W/Z(+\text{jets})$ production, uncertainties due to scale variations are typically about 5-10%, but they can increase up to about 25% in the high- p_{\perp} region of jet production, where higher jet multiplicities become relevant. In Higgs production processes scale uncertainties tend to be significantly larger, by at least a factor of 2, which is indicative of large higher-order corrections.
- **Underlying event corrections and uncertainties**
Multiple parton interactions tend to increase jet production rates, and they have a particularly large influence on observables which are sensitive to high jet multiplicities, like H_T . They typically do not affect inclusive observables, with changes of about 5% or below. Their associated uncertainty is small.
- **Hadronisation corrections and uncertainties**
Hadronisation corrections are similar in magnitude to parton-shower and multiple-scattering effects. The associated uncertainties are about 5%, except for observables such as jet masses, where they can increase to about 20%.

Let us now turn to the uncertainties induced by the NLO+PS matching. As pointed out in Secs. 2 and 3 in order to link R and B in the POWHEG method a combined phase space, helicity and flavour map is needed. One of the obstacles is that, when using the Catani–Seymour method of infrared subtraction, one configuration in R leads to various underlying configurations in B. Conversely, the same configuration in B leads to various possible real emission configurations. In processes of the type $q\bar{q} \rightarrow Z$ or $q\bar{q} \rightarrow VV'$ and similar this is just a minor complication. However, we found that in processes with extra emissions such as $Z + j$ or $W + j$ there is a sizable fraction of events, where some of the contributions emerging from the mapping fail phase space cuts, often leading to an incomplete cancellation of logarithmically enhanced terms, and therefore introducing large numerical instabilities. Due to the absence of a detailed description of these mappings in previous publications, it can only be speculated about the severity of this problem when using the Frixione–Kunszt–Signer subtraction.

Regarding the problem of infrared divergences in sub-leading colour configurations, it should be noted that up to now, only one critical process – heavy quark pair production – has been implemented in a publicly available and fully documented event generator. In this case the problem was solved by introducing a factor that modifies the parton-shower motivated subtraction kernels such that they include the full structure of the soft divergences. A similar strategy seems to be employed in the recently presented aMC@NLO code, but it has not been published or made publicly available yet. It is therefore not yet clear whether this technique is sufficiently process-independent to allow for a general implementation of MC@NLO. In this publication a different approach has been followed, which rather aims at constructing a tractable and correct solution, irrespective of the process considered. This is possible because the parton shower used here is based on the Catani–Seymour subtraction kernels which incorporate the full colour structure in a way that can easily be deconstructed. The basic idea is to correct the Casimir operators used in the parton shower such that the full colour structure in the soft-gluon limit is obtained. This introduces both positive and negative splitting functions, which is unproblematic for NLO calculation but implies “anti-probabilistic” evolution in a parton shower. To resolve this issue, a weighting procedure has been introduced. It is anticipated that this modification will eventually allow the systematic inclusion of sub-leading colour terms in the parton shower.

Regarding the scale choices in both MC@NLO and POWHEG it should be noted that the running of the factorisation and renormalisation scale with each emission, as in the parton shower, is somewhat at odds with the logic intrinsic to a fixed order calculation. In this publication the problem is only noted, and no proper general solution is proposed.

The last point, regarding exponentiation of non-leading terms in MC@NLO and POWHEG is an issue that has been known for some time. Actual differences in how the two methods predict the p_\perp spectrum of the Higgs boson are documented in the literature [25]. They have typically been attributed to a different treatment of higher order, in particular NNLO, corrections (see Sec. 4.3 of [25]). We find that the difference is related to exponentiation uncertainties, naturally affecting the next-to-next-to leading order, but continuing to all orders. The no-emission probability contains logarithms of ratios between the scale related to the upper phase space boundary and the actual transverse momentum of the emission. For the original POWHEG method, the upper boundary is related to the total hadronic centre-of-mass energy, which is substantially different from the scale typically used in resummation programs, such as HqT [53], where a value of the order of the Higgs boson mass is assumed. It is thus clear that a suitable constraint on the emission phase space in POWHEG must be defined. On a related note, the occurrence of the well-known dip around zero in the MC@NLO simulation of the $y_j - y_H$ distribution, the rapidity difference of Higgs boson and accompanying jet, has been studied. Cutting on the phase space of the Catani–Seymour subtraction kernels and reflecting these cuts in the parton shower, as enforced by MC@NLO, yields dead zones of parton emission in the latter. While these dead zones are clearly different from the dead zones in the HERWIG parton shower, the resulting effect is surprisingly similar. In fact, both including the full phase space and comparably tight cuts on the phase space leads to a vanishing dip; this finding suggests that also the dip, which is of course not present in the NLO calculation, must be attributed to the exponentiation in unwanted regions of the emission phase space. The obvious solution for MC@NLO is to ensure that only logarithms related to emissions on scales below the factorisation scale are exponentiated. To this end, physically more meaningful cuts on the phase space of Catani–Seymour subtraction kernels are currently investigated. Devising a similar technology for POWHEG would result in two formally completely equivalent algorithms, but imply a larger computational effort for event generation in POWHEG due to the additional numerical integration in \bar{B} and the matrix-element correction of the weighted parton shower, see [15]. For this reason, in favour of the MC@NLO method, the further development of POWHEG methods in the SHERPA framework will be abandoned.

Acknowledgements

SH's work was supported by the US Department of Energy under contract DE-AC02-76SF00515, in part by the US National Science Foundation, grant NSF-PHY-0705682, (The LHC Theory Initiative), and in part by the US National Science Foundation under grant NSF-PHY-0551164. MS's work was supported by the Research Executive Agency (REA) of the European Union under the Grant Agreement number PITN-GA-2010-264564 (LHCPhenoNet). FS's work was supported by the German Research Foundation (DFG) via grant DI 784/2-1.

The authors would like to thank Massimiliano Grazzini and Stefano Catani for fruitful discussion. FK would also like to thank the Galileo Galilei Institute in Florence and the SLAC theory group for their hospitality while this work was finished. SH thanks the CP³-Origins Odense for hospitality.

References

- [1] S. Catani, F. Krauss, R. Kuhn and B. R. Webber, *QCD matrix elements + parton showers*, JHEP **11** (2001), 063, [[hep-ph/0109231](#)]; M. L. Mangano, M. Moretti and R. Pittau, *Multijet matrix elements and shower evolution in hadronic collisions: $Wb\bar{b} + n$ -jets as a case study*, Nucl. Phys. **B632** (2002), 343–362, [[hep-ph/0108069](#)]; F. Krauss, *Matrix elements and parton showers in hadronic interactions*, JHEP **0208** (2002), 015, [[hep-ph/0205283](#)]; L. Lönnblad, *Correcting the colour-dipole cascade model with fixed order matrix elements*, JHEP **05** (2002), 046, [[hep-ph/0112284](#)]; M. L. Mangano, M. Moretti, F. Piccinini and M. Treccani, *Matching matrix elements and shower evolution for top-pair production in hadronic collisions*, JHEP **01** (2007), 013, [[hep-ph/0611129](#)]; N. Lavesson and L. Lönnblad, *Merging parton showers and matrix elements – back to basics*, JHEP **04** (2008), 085, [[arXiv:0712.2966 \[hep-ph\]](#)]; J. Alwall et al., *Comparative study of various algorithms for the merging of parton showers and matrix elements in hadronic collisions*, Eur. Phys. J. **C53** (2008), 473–500, [[arXiv:0706.2569 \[hep-ph\]](#)]; S. Höche, F. Krauss, S. Schumann and F. Siegert, *QCD matrix elements and truncated showers*, JHEP **05** (2009), 053, [[arXiv:0903.1219 \[hep-ph\]](#)]; K. Hamilton, P. Richardson and J. Tully, *A modified CKKW matrix element merging approach to angular-ordered parton showers*, JHEP **11** (2009), 038, [[arXiv:0905.3072 \[hep-ph\]](#)]; T. Carli, T. Gehrmann and S. Höche, *Hadronic final states in deep-inelastic scattering with SHERPA*, Eur. Phys. J. **C67** (2010), 73, [[arXiv:0912.3715 \[hep-ph\]](#)]; L. Lönnblad and S. Prestel, *Matching Tree-Level Matrix Elements with Interleaved Showers*, [arXiv:1109.4829 \[hep-ph\]](#).
- [2] S. Frixione and B. R. Webber, *Matching NLO QCD computations and parton shower simulations*, JHEP **06** (2002), 029, [[hep-ph/0204244](#)].
- [3] P. Nason, *A new method for combining NLO QCD with shower Monte Carlo algorithms*, JHEP **11** (2004), 040, [[hep-ph/0409146](#)]; S. Frixione, P. Nason and C. Oleari, *Matching NLO QCD computations with parton shower simulations: the POWHEG method*, JHEP **11** (2007), 070, [[arXiv:0709.2092 \[hep-ph\]](#)].
- [4] M. H. Seymour, *Matrix-element corrections to parton shower algorithms*, Comp. Phys. Commun. **90** (1995), 95–101, [[hep-ph/9410414](#)]; M. H. Seymour, *A simple prescription for first-order corrections to quark scattering and annihilation processes*, Nucl. Phys. **B436** (1995), 443–460, [[hep-ph/9410244](#)]; J. André and T. Sjöstrand, *Matching of matrix elements and parton showers*, Phys. Rev. **D57** (1998), 5767–5772, [[hep-ph/9708390](#)]; E. Norrbin and T. Sjöstrand, *QCD radiation off heavy particles*, Nucl. Phys. **B603** (2001), 297–342, [[hep-ph/0010012](#)].
- [5] S. Alioli, K. Hamilton, P. Nason, C. Oleari and E. Re, *Jet pair production in POWHEG*, JHEP **1104** (2011), 081, [[arXiv:1012.3380 \[hep-ph\]](#)].
- [6] S. Alioli, P. Nason, C. Oleari and E. Re, *Vector boson plus one jet production in POWHEG*, JHEP **1101** (2011), 095, [[arXiv:1009.5594 \[hep-ph\]](#)].
- [7] C. Oleari and L. Reina, *$W b \bar{b}$ production in POWHEG*, JHEP **1108** (2011), 061, [[arXiv:1105.4488 \[hep-ph\]](#)].
- [8] R. Frederix, S. Frixione, V. Hirschi, F. Maltoni, R. Pittau and P. Torrielli, *W and Z/γ^* boson production in association with a bottom-antibottom pair*, JHEP **1109** (2011), 061, [[arXiv:1106.6019 \[hep-ph\]](#)].

- [9] R. Frederix, S. Frixione, V. Hirschi, F. Maltoni, R. Pittau and P. Torrielli, *aMC@NLO predictions for Wjj production at the Tevatron*, [arXiv:1110.5502](#) [hep-ph].
- [10] G. Aad et al., The ATLAS collaboration, *Search for squarks and gluinos using final states with jets and missing transverse momentum with the ATLAS detector in $\sqrt{s} = 7$ TeV proton-proton collisions*, Phys.Lett. **B701** (2011), 186–203, [[arXiv:1102.5290](#) [hep-ex]]; G. Aad et al., The ATLAS collaboration, *Search for supersymmetry using final states with one lepton, jets, and missing transverse momentum with the ATLAS detector in $\sqrt{s} = 7$ TeV pp* , Phys.Rev.Lett. **106** (2011), 131802, [[arXiv:1102.2357](#) [hep-ex]]; S. Chatrchyan et al., The CMS collaboration, *Search for New Physics with a Mono-Jet and Missing Transverse Energy in pp Collisions at $\sqrt{s} = 7$ TeV*, [arXiv:1106.4775](#) [hep-ex]; S. Chatrchyan et al., The CMS collaboration, *Search for New Physics with Jets and Missing Transverse Momentum in pp collisions at $\sqrt{s} = 7$ TeV*, [arXiv:1106.4503](#) [hep-ex]; S. Chatrchyan et al., The CMS collaboration, *Search for supersymmetry in pp collisions at $\sqrt{s}=7$ TeV in events with a single lepton, jets, and missing transverse momentum*, [arXiv:1107.1870](#) [hep-ex].
- [11] G. Aad et al., The ATLAS collaboration, *Measurement of the production cross section for W -bosons in association with jets in pp collisions at $\sqrt{s} = 7$ TeV with the ATLAS detector*, Phys.Lett. **B698** (2011), 325–345, [[arXiv:1012.5382](#) [hep-ex]].
- [12] G. Aad et al., The ATLAS collaboration, *A measurement of the ratio of the W and Z cross sections with exactly one associated jet in pp collisions at $\sqrt{s} = 7$ TeV with ATLAS*, [arXiv:1108.4908](#) [hep-ex]; S. Ask, The ATLAS collaboration, *Measurement of the production cross section for W - and Z -bosons in association with jets in ATLAS*, [arXiv:1106.2061](#) [hep-ex]; S. Chatrchyan et al., The CMS collaboration, *Measurement of the Polarization of W Bosons with Large Transverse Momenta in W +Jets Events at the LHC*, Phys. Rev. Lett. **107** (2011), 021802, [[arXiv:1104.3829](#) [hep-ex]]; C. Rogan, The CMS collaboration, *W +jets and Z +jets studies with the CMS detector at the CERN LHC*, PoS **HCP2009** (2009), 096.
- [13] J. M. Campbell and R. Ellis, *Next-to-leading order corrections to $W^+ 2$ jet and $Z^+ 2$ jet production at hadron colliders*, Phys.Rev. **D65** (2002), 113007, [[arXiv:hep-ph/0202176](#) [hep-ph]]; R. Ellis, K. Melnikov and G. Zanderighi, *$W + 3$ jet production at the Tevatron*, Phys.Rev. **D80** (2009), 094002, [[arXiv:0906.1445](#) [hep-ph]]; R. Ellis, K. Melnikov and G. Zanderighi, *Generalized unitarity at work: first NLO QCD results for hadronic $W^+ 3$ jet production*, JHEP **0904** (2009), 077, [[arXiv:0901.4101](#) [hep-ph]].
- [14] C. F. Berger, Z. Bern, L. J. Dixon, F. Febres-Cordero, D. Forde, H. Ita, D. A. Kosower and D. Maître, *Automated implementation of on-shell methods for one-loop amplitudes*, Phys.Rev. **D78** (2008), 036003, [[arXiv:arXiv:0803.4180](#) [hep-ph]]; C. F. Berger, Z. Bern, L. J. Dixon, F. Febres-Cordero, D. Forde, T. Gleisberg, H. Ita, D. A. Kosower and D. Maître, *Precise Predictions for $W + 3$ Jet Production at Hadron Colliders*, Phys. Rev. Lett. **102** (2009), 222001, [[arXiv:0902.2760](#) [hep-ph]]; C. F. Berger, Z. Bern, L. J. Dixon, F. Febres-Cordero, D. Forde, T. Gleisberg, H. Ita, D. A. Kosower and D. Maître, *Next-to-leading order QCD predictions for $Z, \gamma^* + 3$ -Jet distributions at the Tevatron*, Phys. Rev. **D82** (2010), 074002, [[arXiv:1004.1659](#) [hep-ph]]; C. F. Berger, Z. Bern, L. J. Dixon, F. Febres-Cordero, D. Forde, T. Gleisberg, H. Ita, D. A. Kosower and D. Maître, *Precise Predictions for $W + 4$ -Jet Production at the Large Hadron Collider*, Phys.Rev.Lett. **106** (2011), 092001, [[arXiv:1009.2338](#) [hep-ph]]; H. Ita, Z. Bern, L. J. Dixon, F. Febres-Cordero, D. A. Kosower and D. Maître, *Precise Predictions for $Z + 4$ Jets at Hadron Colliders*, [arXiv:1108.2229](#) [hep-ph].
- [15] S. Höche, F. Krauss, M. Schönherr and F. Siegert, *Automating the POWHEG method in SHERPA*, JHEP **04** (2011), 024, [[arXiv:1008.5399](#) [hep-ph]].
- [16] S. Catani and M. H. Seymour, *A general algorithm for calculating jet cross sections in NLO QCD*, Nucl. Phys. **B485** (1997), 291–419, [[hep-ph/9605323](#)]; S. Catani, S. Dittmaier, M. H. Seymour and Z. Trocsanyi, *The dipole formalism for next-to-leading order QCD calculations with massive partons*, Nucl. Phys. **B627** (2002), 189–265, [[hep-ph/0201036](#)].
- [17] S. Frixione, Z. Kunszt and A. Signer, *Three-jet cross-sections to next-to-leading order*, Nucl. Phys. **B467** (1996), 399–442, [[hep-ph/9512328](#)]; S. Frixione, *A general approach to jet cross sections in QCD*, Nucl. Phys. **B507** (1997), 295–314, [[hep-ph/9706545](#)].

- [18] K. Mikaelian, M. Samuel and D. Sahdev, *The Magnetic Moment of Weak Bosons Produced in $p p$ and p anti- p Collisions*, Phys.Rev.Lett. **43** (1979), 746, Research Note 86; C. Goebel, F. Halzen and J. Leveille, *Angular zeros of Brown, Mikaelian, Sahdev, and Samuel and the factorization of tree amplitudes in gauge theories*, Phys.Rev. **D23** (1981), 2682–2685; Z. Bern, J. Carrasco and H. Johansson, *New Relations for Gauge-Theory Amplitudes*, Phys.Rev. **D78** (2008), 085011, [[arXiv:0805.3993](#) [hep-ph]].
- [19] S. Alioli, P. Nason, C. Oleari and E. Re, *NLO vector-boson production matched with shower in POWHEG*, JHEP **07** (2008), 060, [[arXiv:0805.4802](#) [hep-ph]].
- [20] S. Frixione, P. Nason and B. R. Webber, *Matching NLO QCD and parton showers in heavy flavour production*, JHEP **08** (2003), 007, [[hep-ph/0305252](#)].
- [21] R. Frederix, private communication.
- [22] Y. L. Dokshitzer, D. Diakonov and S. I. Troian, *Hard Processes in Quantum Chromodynamics*, Phys. Rept. **58** (1980), 269–395.
- [23] A. Buckley et al., *General-purpose event generators for LHC physics*, Phys. Rept. **504** (2011), 145–233, [[arXiv:1101.2599](#) [hep-ph]].
- [24] S. Alioli, P. Nason, C. Oleari and E. Re, *A general framework for implementing NLO calculations in shower Monte Carlo programs: the POWHEG BOX*, JHEP **06** (2010), 043, [[arXiv:1002.2581](#) [hep-ph]].
- [25] S. Alioli, P. Nason, C. Oleari and E. Re, *NLO Higgs boson production via gluon fusion matched with shower in POWHEG*, JHEP **04** (2009), 002, [[arXiv:0812.0578](#) [hep-ph]].
- [26] T. Gleisberg and F. Krauss, *Automating dipole subtraction for QCD NLO calculations*, Eur. Phys. J. **C53** (2008), 501–523, [[arXiv:0709.2881](#) [hep-ph]].
- [27] S. Schumann and F. Krauss, *A parton shower algorithm based on Catani-Seymour dipole factorisation*, JHEP **03** (2008), 038, [[arXiv:0709.1027](#) [hep-ph]].
- [28] T. Plehn, D. Rainwater and P. Skands, *Squark and gluino production with jets*, Phys. Lett. **B645** (2007), 217–221, [[hep-ph/0510144](#)]; R. Corke and T. Sjöstrand, *Improved Parton Showers at Large Transverse Momenta*, Eur. Phys. J. **C69** (2010), 1–18, [[arXiv:1003.2384](#) [hep-ph]].
- [29] S. Alioli, K. Hamilton and E. Re, *Practical improvements and merging of POWHEG simulations for vector boson production*, [arXiv:1108.0909](#) [hep-ph].
- [30] S. Höche, F. Krauss, M. Schönherr and F. Siegert, *NLO matrix elements and truncated showers*, JHEP **08** (2011), 123, [[arXiv:1009.1127](#) [hep-ph]].
- [31] S. Höche, S. Schumann and F. Siegert, *Hard photon production and matrix-element parton-shower merging*, Phys. Rev. **D81** (2010), 034026, [[arXiv:0912.3501](#) [hep-ph]].
- [32] S. Platzer and M. Sjöstrand, *The Sudakov Veto Algorithm Reloaded*, [arXiv:1108.6180](#) [hep-ph].
- [33] T. Sjöstrand, S. Mrenna and P. Skands, *PYTHIA 6.4 physics and manual*, JHEP **05** (2006), 026, [[hep-ph/0603175](#)].
- [34] T. Gleisberg, S. Höche, F. Krauss, A. Schälicke, S. Schumann and J. Winter, *SHERPA 1.0, a proof-of-concept version*, JHEP **02** (2004), 056, [[hep-ph/0311263](#)]; T. Gleisberg, S. Höche, F. Krauss, M. Schönherr, S. Schumann, F. Siegert and J. Winter, *Event generation with SHERPA 1.1*, JHEP **02** (2009), 007, [[arXiv:0811.4622](#) [hep-ph]].
- [35] F. Krauss, R. Kuhn and G. Soff, *AMEGIC++ 1.0: A Matrix Element Generator In C++*, JHEP **02** (2002), 044, [[hep-ph/0109036](#)].
- [36] P. M. Nadolsky et al., *Implications of CTEQ global analysis for collider observables*, Phys. Rev. **D78** (2008), 013004, [[arXiv:0802.0007](#) [hep-ph]].
- [37] A. Buckley et al., *Rivet user manual*, [arXiv:1003.0694](#) [hep-ph].

- [38] S. Catani, Y. L. Dokshitzer, M. H. Seymour and B. R. Webber, *Longitudinally-invariant k_{\perp} -clustering algorithms for hadron-hadron collisions*, Nucl. Phys. **B406** (1993), 187–224; S. D. Ellis and D. E. Soper, *Successive combination jet algorithm for hadron collisions*, Phys. Rev. **D48** (1993), 3160–3166, [[hep-ph/9305266](#)]; M. Cacciari and G. P. Salam, *Dispelling the N^3 myth for the k_t jet-finder*, Phys. Lett. **B641** (2006), 57–61, [[hep-ph/0512210](#)].
- [39] S. Dawson, *Radiative corrections to Higgs boson production*, Nucl. Phys. **B359** (1991), 283–300; A. Djouadi, M. Spira and P. Zerwas, *Production of Higgs bosons in proton colliders: QCD corrections*, Phys.Lett. **B264** (1991), 440–446.
- [40] Z. Nagy, *Next-to-leading order calculation of three-jet observables in hadron-hadron collisions*, Phys. Rev. **D68** (2003), 094002, [[hep-ph/0307268](#)].
- [41] J. Campbell and R. K. Ellis, *MCFM – Monte Carlo for FeMtobarn processes*; V. Ravindran, J. Smith and W. Van Neerven, *Next-to-leading order QCD corrections to differential distributions of Higgs boson production in hadron-hadron collisions*, Nucl.Phys. **B634** (2002), 247–290, [[hep-ph/0201114](#)].
- [42] J.-C. Winter, F. Krauss and G. Soff, *A modified cluster-hadronisation model*, Eur. Phys. J. **C36** (2004), 381–395, [[hep-ph/0311085](#)]; F. Krauss et al., *SHERPA’s new hadronisation model*, in preparation.
- [43] T. Sjöstrand and M. van Zijl, *A multiple-interaction model for the event structure in hadron collisions*, Phys. Rev. **D36** (1987), 2019; S. Alekhin et al., *HERA and the LHC - A workshop on the implications of HERA for LHC physics: Proceedings Part A*, [hep-ph/0601012](#).
- [44] F. Krauss, T. Laubrich and F. Siegert, *Simulation of hadron decays in SHERPA*, in preparation.
- [45] M. Schönherr and F. Krauss, *Soft photon radiation in particle decays in SHERPA*, JHEP **12** (2008), 018, [[arXiv:0810.5071 \[hep-ph\]](#)].
- [46] B. Andersson, G. Gustafson, G. Ingelman and T. Sjöstrand, *Parton Fragmentation and String Dynamics*, Phys. Rept. **97** (1983), 31–145; B. Andersson, *The Lund model*, vol. 7, Camb. Monogr. Part. Phys. Nucl. Phys. Cosmol., 1997.
- [47] T. Aaltonen et al., The CDF collaboration, *Measurement of Inclusive Jet Cross Sections in $Z/\gamma^*(\rightarrow ee)+jets$ Production in $p\bar{p}$ Collisions at $\sqrt{s} = 1.96$ TeV*, Phys. Rev. Lett. **100** (2008), 102001, [[arXiv:0711.3717 \[hep-ex\]](#)].
- [48] A. Abulencia et al., The CDF collaboration, *Measurement of the inclusive jet cross section in $p\bar{p}$ interactions at $\sqrt{s} = 1.96$ -TeV using a cone-based jet algorithm.*, Phys.Rev. **D74** (2006), 071103, [[hep-ex/0512020](#)].
- [49] V. M. Abazov et al., The DØ collaboration, *Measurement of differential $Z/\gamma^* + jet + X$ cross sections in $p\bar{p}$ collisions at $\sqrt{s} = 1.96$ TeV*, Phys. Lett. **B669** (2008), 278–286, [[arXiv:0808.1296 \[hep-ex\]](#)].
- [50] G. C. Blazey et al., *Run II jet physics*, [hep-ex/0005012](#).
- [51] V. Abazov et al., The DØ collaboration, *Measurements of differential cross sections of $Z/\gamma^*+jets+X$ events in proton anti-proton collisions at $\sqrt{s} = 1.96$ TeV*, Phys.Lett. **B678** (2009), 45–54, [[arXiv:0903.1748 \[hep-ex\]](#)].
- [52] V. M. Abazov et al., The DØ collaboration, *Measurement of $Z/\gamma^*+jet+X$ angular distributions in $p\bar{p}$ collisions at $\sqrt{s} = 1.96$ TeV*, Phys. Lett. **B682** (2010), 370–380, [[arXiv:0907.4286 \[hep-ex\]](#)].
- [53] D. de Florian, G. Ferrera, M. Grazzini and D. Tommasini, *Transverse-momentum resummation: Higgs boson production at the Tevatron and the LHC*, [arXiv:1109.2109 \[hep-ph\]](#).